8-2005

Determination and Comparison of In Vivo Forces and Torques in Normal and Degenerative Lumbar Spines

Shaun Kevin Stinton
University of Tennessee - Knoxville

To the Graduate Council:

I am submitting herewith a thesis written by Shaun Kevin Stinton entitled "Determination and Comparison of In Vivo Forces and Torques in Normal and Degenerative Lumbar Spines." I have examined the final electronic copy of this thesis for form and content and recommend that it be accepted in partial fulfillment of the requirements for the degree of Master of Science, with a major in Engineering Science.

Richard D. Komistek, Major Professor

We have read this thesis and recommend its acceptance:

Jack F. Wasserman, Mohamed R. Mahfouz

Accepted for the Council:
Carolyn R. Hodges

Vice Provost and Dean of the Graduate School

(Original signatures are on file with official student records.)

To the Graduate Council:

I am submitting herewith a thesis written by Shaun Kevin Stinton entitled "Determination and Comparison of In Vivo Forces and Torques in Normal and Degenerative Lumbar Spines." I have examined the final electronic copy of this thesis for form and content and recommend that it be accepted in partial fulfillment of the requirements for the degree of Master of Science, with a major in Engineering Science.

Richard D. Komistek

Major Professor

We have read this thesis

and recommend its acceptance:

Jack F. Wasserman

Mohamed R. Mahfouz

Acceptance for the Council:

Anne Mayhew

Vice Chancellor and Dean of

Graduate Studies

(Original signatures on file with official student records.)

Determination and Comparison of In Vivo Forces and Torques in Normal and Degenerative Lumbar Spines

A Thesis

Presented for the

Masters of Science Degree

The University of Tennessee, Knoxville

Shaun Kevin Stinton
August, 2005

DEDICATION

This thesis is dedicated to my family and friends who were very understanding during the times when I disappeared for weeks or months at a time while working on various projects and on this thesis.

ACKNOWLEDGEMENTS

I would like to thank Dr. Komistek for giving me the opportunity to work on this project and for his guidance. I would also like to thank Dr. Mahfouz and Dr. Wasserman for their help and for being on my thesis committee.

I would also like to thank Scott Walker, Matt Anderle, and the other graduate students whose friendships outside of the lab were more rewarding than all of the assistance they provided within the lab.

ABSTRACT

In vivo motions of normal and degenerative lumbar spine patients performing extension/flexion were obtained using video fluoroscopy. 3-D models of each patient's vertebrae were registered to the 2-D fluoroscopy images using a process developed at Rocky Mountain Musculoskeletal Research Laboratory. Temporal equations representing the motions were input into a math model and the forces at the contact point between vertebral levels and the body torques between the vertebrae were the output. The vertical forces in the normal and degenerative patients were similar and ranged from 0.35-0.42 times the body weight of the patient. The maximum torques were higher in the degenerative patient than in the normal patient. The maximum torques between L4 and L5 were 11.1 N*m in the degenerative patient and 9.72 N*m in the normal patient. At L3/L4, the maximum torque was 10.3 N*m in the degenerative and 9.03 N*m in the normal patient. The maximum torques in the degenerative patient were also higher than in the normal patient at the L2/L3 and L1/L2 levels. Left untreated these higher torques could cause deterioration of other levels as the spine tries to compensate for existing degenerative levels. This model will lead to a better understanding of the lumbar spine and could aid in treating lower back pain and in the design of spinal prostheses.

TABLE OF CONTENTS

LIST OF FIGURES

1 INTRODUCTION

1.1 Anatomy

The lumbar spine consists of five lumbar vertebrae, the sacrum and the coccyx (Figure 1-1). Each vertebra is connected to each adjacent vertebral body by three joints, one anterior (vertebral disc) and two posterior (facet joints) (Figure 1-1). The soft tissues associated with the lumbar spine are the intervertebral discs, the facet joint capsules, ligaments, and muscles (Figure 1-2). The roles of the spine are to support weight, maintain balance, control movement, counter the numerous daily strains that are exerted on it during normal recreational and working activities, and to protect the neural elements (Niosi and Oxland, 2004). Although it has tremendous ability to withstand most mechanical stresses, failure of some tissues may occur when these stresses exceed the limits of various spinal structures. Consequently, this may result in the genesis of pain and also reduction of the spine's capacity to resist these forces. The most dehabilitating pain within the spine often occurs in the lumbar spine, which can lead to the common problem of lower back pain (LBP).

1.2 Low Back Pain

The most common spine related problem is lower back pain. It is estimated that 80-90% of the U.S. population will experience lower back pain at some point in their lifetime. It is the most common work-related medical problem in the United States, and

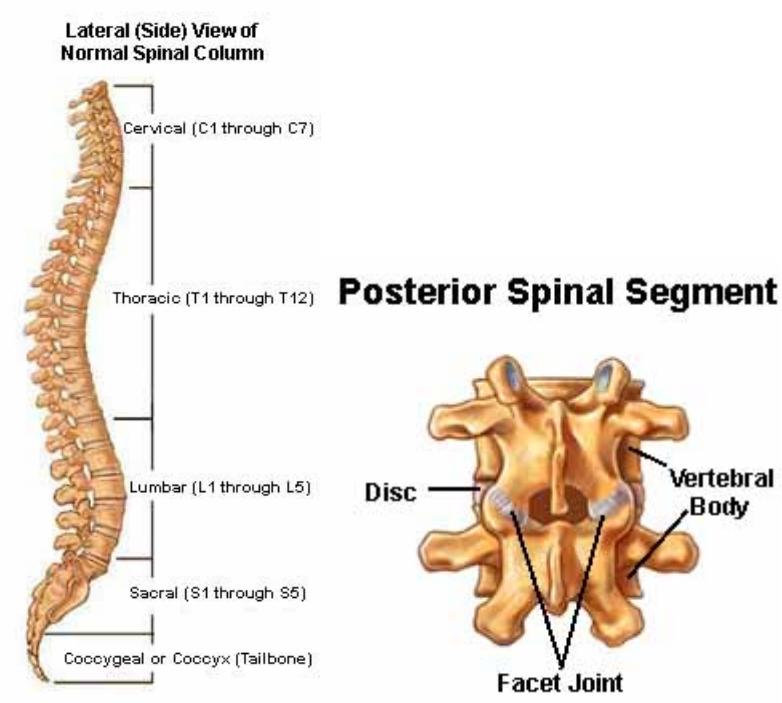

Figure 1-1. Diagram showing the 5 lumbar vertebra, sacrum and coccyx (Left) 3 joint system of intervertebral disc and facet joints (Right) – pictures from spineuniverse.com

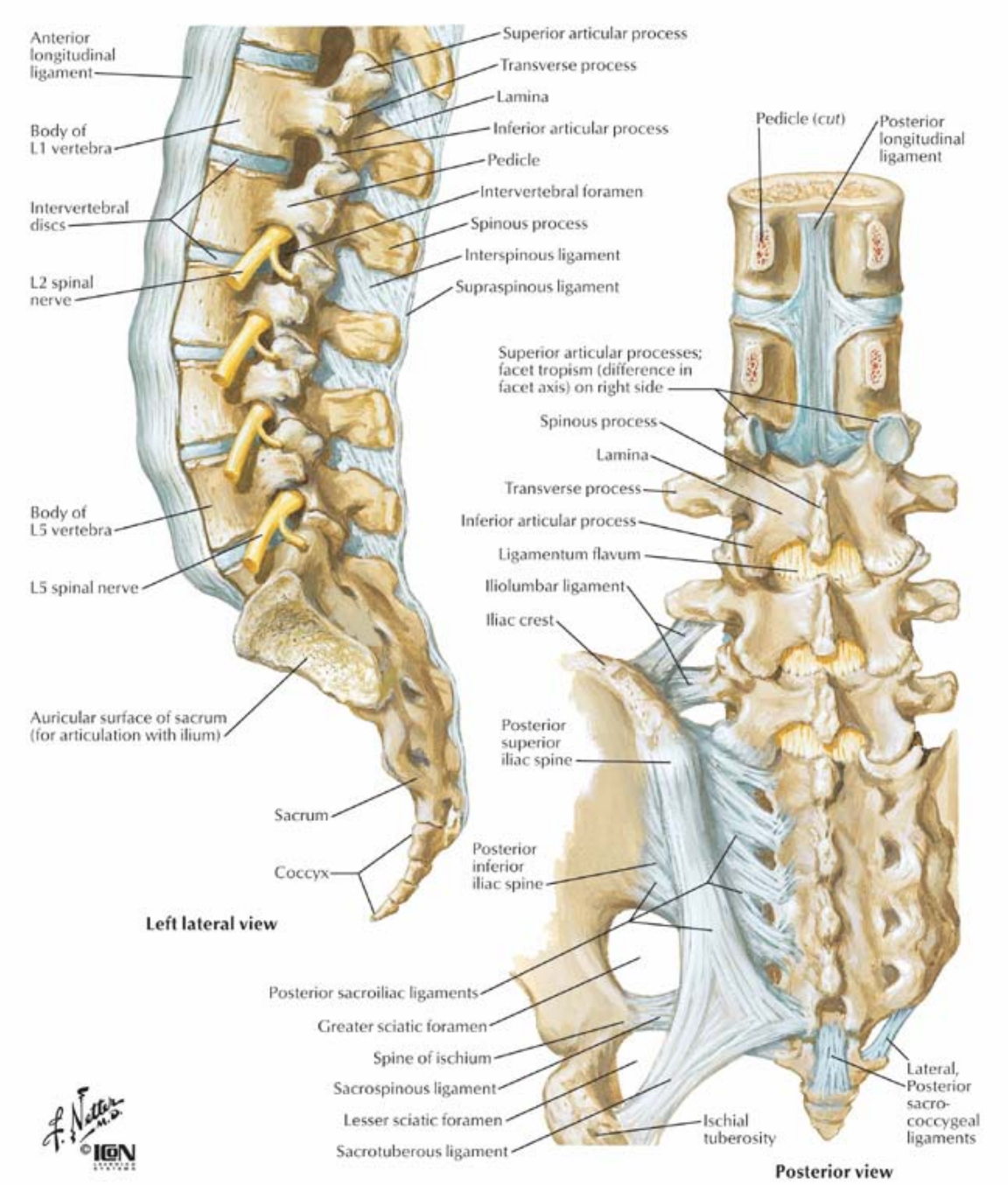

Figure 1-2. Section of the lumbar spine showing anatomy of bone, muscles, ligaments and nerves. – picture from http://www.backpain-guide.com

the second most common reason for doctor visits behind the common cold. Lower back pain is the leading cause of disability among people ages 19-45 and is the leading cause of missed work days. People with chronic back pain account for 80% of the cost of treatment in workers compensation claims. Longer life-spans and an increasing proportion of middle aged and elderly people make lower back pain an increasingly significant problem. The cost in terms of treatments and missed work is billions of dollars annually. (National Center for Health Statistics; Roberts, 1993; Weinstein, 1993; Taylor et al., 1994; Luo et al., 2004, World Health Organization; Kelsey and White, 1980)

Bone strength and muscle elasticity decreases as a person ages. Intervertebral discs begin to lose fluid and flexibility, which decreases their ability to cushion the vertebrae. Pain can occur when someone lifts something too heavy or overstretches, causing a sprain, strain, or spasm in one of the muscles or ligaments in the back. If the spine becomes overly strained or compressed, a disc may rupture or bulge outward. This rupture may put pressure on one of the nerves connected to the spinal cord. The pain results from the irritation of the nerves.

A majority of back pain is due to injury or trauma to the back, but degenerative conditions such as arthritis or disc disease, osteoporosis or other bone diseases, viral infections, irritation to joints and discs, and cancer can also cause lower back pain. Obesity, smoking, weight gain during pregnancy, stress, poor physical condition, poor posture, and poor sleeping position are factors that can increase the risk of low back pain. Scar tissue created from previous back injuries does not have the strength or flexibility of normal tissue which can lead to future injury.

Lower back pain can also be a sign of a more serious medical problem. Pain accompanied by fever or loss of bowel or bladder control, pain when coughing, and progressive weakness in the legs may indicate a pinched nerve, diabetes, or another serious condition. (National Institute for Neurological Disorder and Stroke)

All back pain in the region of the lumbar spine is classified as lower back pain. Currently, it is hard to specifically classify lower back pain which leads to difficulty in diagnosing and treating different types of pain. A mathematical model of the lumbar spine could help in diagnosis and treatment of lower back pain because the model will lead to a better understanding of back pain by determining the *in vivo* interactive contact forces and torques that occur in the lumbar vertebrae during an active movement. The forces and torques in normal and degenerative lumbar spines could be compared using the model to aid in determining the cause of lumbar spine pain and degeneration. Knowledge of the forces and motions associated with the lumbar spine could also be used in future design of spinal prostheses including lumbar disc replacements and facet joint replacements by providing a knowledge of the forces and torques that the prostheses will need to withstand *in vivo*. Therefore, the objective of this present study was to derive a three-dimensional mathematical model of the human lumbar spine system to determine the in vivo forces at the bearing surface interface and the in vivo torques across rigid body segments.

1.3 Treatment

Non-surgical methods are the first treatments used for lower back pain. Medications including non-steroidal anti-inflammatory drugs, muscle relaxants, and

epidural steroid injections may be used to control pain and reduce inflammation and muscle spasms. Physical therapy using ice treatments, heat treatments, ultrasound and chiropractic braces are also used to treat lower back pain without surgery. Manipulation of the spine (chiropractics) and traction are also used. Traction involves applying a constant or intermittent force to gradually put the skeletal structure into better alignment. Traction is not recommended for treating acute lower back symptoms. These treatments do not cure the problem of lower back pain, they just treat the symptoms.

Minimally invasive treatments of the vertebrae include vertebroplasty and kyphoplasty. In vertebroplasty a doctor guides a needle into the vertebral body with the aid of imaging (usually fluoroscopy). A glue-like epoxy is injected and hardens quickly which stabilizes and strengthens the bone and provides immediate pain relief. In kyphoplasty, prior to injecting an epoxy, a balloon is used. The balloon is inserted and inflated to restore shape to the bone and reduce spinal deformity.

Spinal laminectomy, discectomy, and foraminotomy are all surgeries with the goal of relieving pressure on the spinal cord and relieving pain. Spinal laminectomy (decompression) involves the removal of the lamina which increases the size of the spinal canal thereby relieving pressure on the spinal cord. The outer wall of a disc, called the annulus fibrosis, can tear from injury or weakness due to aging allowing the soft inner part of the disc, the nucleus pulposus, to bulge out. Discectomy involves a small incision in the skin over the spine, the removal of some ligament and bone material and the removal of some of the bulging disc material or bone spur. Foraminotomy enlarges the bony hole where a nerve root exits the spinal canal. Bulging discs or joints thickened with age can cause narrowing of the space through which the spinal nerve exits (spinal

stenosis) causing pain, numbness, and weakness in an arm or leg. Small pieces of bone over the nerve are removed allowing the surgeon to cut away the blockage and relieve the pressure on the nerve.

Other surgical procedures to relieve severe chronic pain include several techniques for blocking the transmission of pain through the nervous system. In these techniques, certain nerve roots, nerve fibers, or neurons are destroyed surgically to prevent the conduction of pain signals. (National Institute for Neurological Disorder and Stroke)

Spinal fusion is used to strengthen the spine and prevent painful movements. A fusion is performed to prevent or correct a deformity, to stabilize the spine, or to relieve chronic pain (Dooris, et. al., 2001). The spinal disc or discs between the vertebrae levels are removed and the adjacent vertebrae are fused using donor bone grafts or bone grafts from the patient's hip. Metal devices secured by screws are sometimes used for better fixation of the fused vertebrae. Spinal fusion results in some loss of flexibility and range of motion in the spine and requires a long recovery period to allow the bone grafts to grow and fuse the vertebrae together.

Artificial disc replacements and total facet replacements are currently being looked at for the future of spine surgery as an improvement over spinal fusion. These methods are favorable because they may provide a method of restoring more normal motions as well as relieving pain. Spinal fusion and other methods or stabilization or fixation of the spine do not allow for natural motion within the spine which may lead to further degeneration in the spine (Etebar and Cahill, 1999; Throckmorton et al., 2003).

1.4 Previous Research

1.4.1 Kinematics

Researchers have previously used several methods to determine kinematics in the human body. These methods include gait lab analysis with skin markers, bone pins, Roentgen Stereophotogrammetric Analysis (RSA), cadaver studies, and fluoroscopy. Skin markers have been used to study various joints in the body (Andriacchi et al., 1998; Soutas-Little et al., 1987). Skin markers have been used by several groups to study kinematics in the lumbar spine (Rowe and White, 1996; Crosbie et al., 1997; Whittle and Levine, 1997). Reflective markers are placed on the skin and tracked using a system of video cameras (Figure 1-3). The cameras have a light source which is directed to the markers which then reflect the light back to the cameras. The markers are placed in specific positions to track bony landmarks. The motion of the markers is tracked throughout the movement.

The main problems with the use of markers to track body kinematics are that identification of standard bony landmarks can be unreliable and that the soft tissue overlying the bony landmarks moves in relation to the underlying bones so the true kinematics of the bone are not being measured (Cheze, 2000; Cappozo, 1991). It has been shown that measurement errors of up to 18 degrees in rotation can be obtained through skin markers (Murphy, 1990). The markers themselves can also move during the movement due to their own inertia.

Figure 1-3. Example of markers used in gait lab analysis.

Bone pins have also been used to obtain *in vivo* kinematics (LaFortune, 1992). Bone pins are an accurate method of obtaining kinematics from patients, but it is a very invasive process that cannot be done on a large number of patients. The error in one bone pin study was found to be less than 0.4 mm (Ramsey et al., 2003).

Roentgen Stereophotogrammetric Analysis originally involved the placement of markers, usually tantalum beads, within the area or interest or within an implant. These markers were studied on the radiographs. More recently, landmarks on the radiographs themselves are tracked. RSA requires manually defining a large number of markers in radiographs, which is a time-consuming process. There can also be errors involved in the manual placements of the markers. The RSA analysis can also be expensive and invasive (Rogers et al., 2005). RSA does not give kinematic results in dynamic motion because

still x-rays are used. RSA has been utilized to determine the stabilizing effects of lumbar fusion or spine implants in several studies (Pape et al., 2000; Gunnarson et al., 2000; Johnsson et al., 1999; Goto et al., 2003).

Cadaver studies allow for physical measurement of motions and forces, but they do not accurately model *in vivo* conditions because it is not possible to identically simulate the *in vivo* conditions in a test setup. The muscles and ligaments do not have the same properties as they do *in vivo* and the method of restraining the vertebrae in the testing setup is not equivalent to *in vivo* conditions. The results from *in vitro* and *in vivo* studies can differ significantly (Rohlmann et al., 1997).

Fluoroscopy has been used more recently by several groups to study kinematics in the knee, hip, shoulder, ankle, spine, and other joints (Dennis et al., 1998; Banks et al., 1996; Hoff et al., 1998). Fluoroscopy combined with a method of 2D to 3D registration allows for accurate and non-invasive measurement of the true, *in vivo* kinematics from dynamic weight bearing activities that can be applied to a large number of patients. Fluoroscopy has been shown to have an error of 0.5° for in-plane translations and less than 0.5 mm for in-plane translations (Mahfouz et al., 2003). A detailed explanation of fluoroscopy is the methods section.

1.4.2 Kinetics

The two methods for determining *in vivo* loads that are most widely used are telemetry and mathematical modeling. Telemetry is the direct measurement of forces at interfaces or measurement of moments across a joint. Telemetry can be very expensive and is technically challenging due to the instrumentation necessary. The sample size is

small due to the expense, and the implanted sensors can fail after implantation which produces no results. Telemetry has been used to determine forces in the hip joint by several groups (Bergmann et al. 1993, 1997; Davy et al. 1998). Telemetry has been used to find forces in the knee joint as well (Taylor et al., 1998; Taylor and Walker, 2001; Kaufman et al., 1996). The use of telemetry in the knee and in other joints has been less successful than in the hip joint.

The use of telemetry in the spine includes animal studies, *in vitro* human studies, and studies that measured the *in vivo* forces on implanted spinal fixation devices. In a study by Ledet et al., sensors were imbedded into the interbody space in the lumbar spine of two baboons. Real-time *in vivo* forces were measured. An interbody spinal implant was fitted with strain gauges and was used as a load cell. The purpose of the study was to compare the forces for various activities and postures. The study found that the forces for standing were 2 times body weight and for standing in flexion the forces were 2.6 times body weight. The results from this study, as well as all animal studies, have to be evaluated cautiously due to the differences in anatomy and physiology between humans and the animals.

In vitro studies using telemetry are a more cost effective method of finding forces in the lumbar spine than *in vivo* methods. The sample sizes in these studies can be larger, but the accuracy of the data is a disadvantage. The test set-up and results for an *in vitro* study may not be very accurate in recreating *in vivo* conditions (Rohlmann et al., 1997).

Nachemson et al. and Rohlmann et al. have done telemetry on human subjects. In the study conducted by Nachemson, distraction rods were telemeterized and the forces were measured to be in the range of 0.29 to 3.86 times body weight depending on the

activity (Nachemson, 1966). Rohlmann et al., implanted spinal fixators across various vertebral levels in 3 patients. The fixators were telemeterized to measure forces. The *in vivo* force results were then compared to previous *in vitro* studies. The forces and torques found in the patients tended to be higher than the forces found in the cadaver tests. The forces found in the 3 patients ranged from 0 to 0.6 times body weight. The bending moments found in the patients were 5 to 10 Newton meters and bending moments in the cadaver studies were slightly lower with the maximum being 6 Newton meters. Force measurements taken with the telemeterized spinal fixation devices are also not the actual forces seen at the interface due to the load sharing between the spine and the implant. (White and Panjabi, 1990).

Mathematical modeling is a theoretical method of determining *in vivo* forces that can be applied to any number of subjects. There are two main approaches to mathematical modeling: optimization to solve an indeterminate muscle force system and reduction to minimize the number of unknowns to keep the number of unknowns equal to the number of equations that can be developed to solve for the unknowns (Komistek et al., 2005). Mathematical models can utilize forward or inverse dynamic methodologies. Forward dynamics outputs kinematics from forces that are input while inverse dynamics uses input kinematics to output forces. Inverse dynamics is the most commonly used approach and involves the experimental determination of motions that are input to a mathematical model used to predict the forces.

1.5 Research Aims

Low back pain is a common problem that is a major expense to the health care industry and to businesses due to the chronic and debilitating nature of the pain. The aim of this study is to bring a greater knowledge of what forces and torques are present in degenerative patients that could lead to low back pain. A better understanding of the forces and torques in the lumbar spine may lead to better methods of diagnosis and treatment for low back pain and will help in defining the design parameters of prostheses and total facet joint replacements. This thesis describes the initial model to predict in vivo contact forces and torques in any patient that has had fluoroscopy and CT scanning.

2 MATERIALS AND METHODS

2.1 Overview

The methodology of the study was to obtain kinematic data from patients with normal and degenerative lumbar spines using fluoroscopy. Then 3D models of each patient's vertebrae were created and registered to the 2D fluoroscopy images to obtain accurate 3D motions through the range of the activity. These motions were the input into a math model which output interactive forces and torques between the lumbar vertebrae (Figure 2-1).

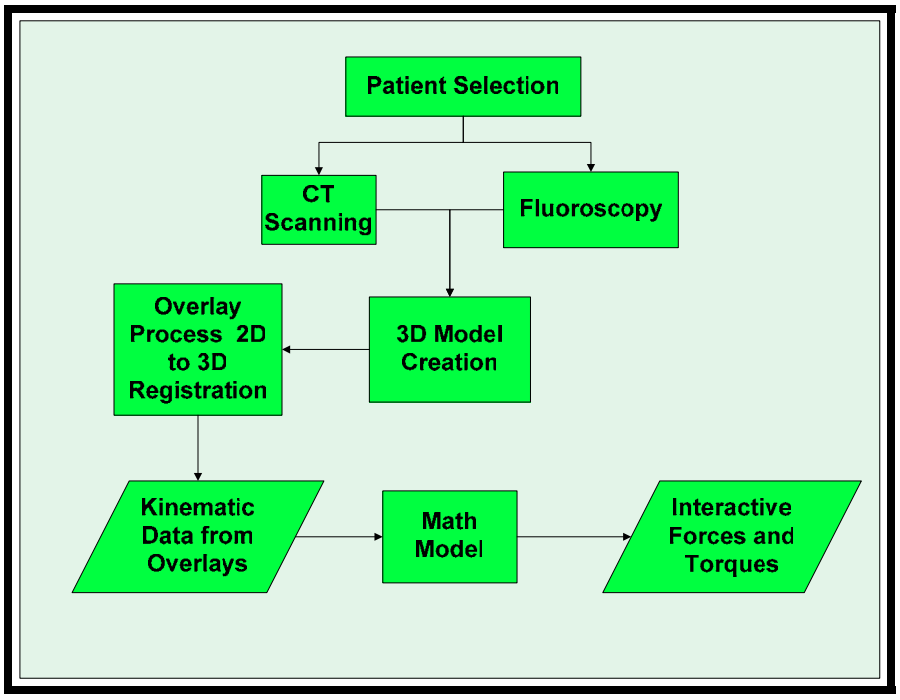

Figure 2-1. Overview of Process.

2.2 Patient Selection

One normal and one degenerative patient were examined in this study. The patients underwent fluoroscopic surveillance and were CT scanned which will be explained in detail in the next sections. The normal patient was a male in his 20's. The degenerative patient was an older male in his 70's. The normal patient had a normal functioning lumbar spine with no reported pain. The degenerative patient was diagnosed with grade I spondylolisthesis of L5 on S1. Spondylolisthesis is a forward slip of a vertebra over the vertebra below it (Figure 2-2). This slippage is often due to a defect in the pars interarticularis. Grade I sponylolisthesis is a congenital dysplasia which in this case is abnormal development of the tissues of the S1 superior facet.

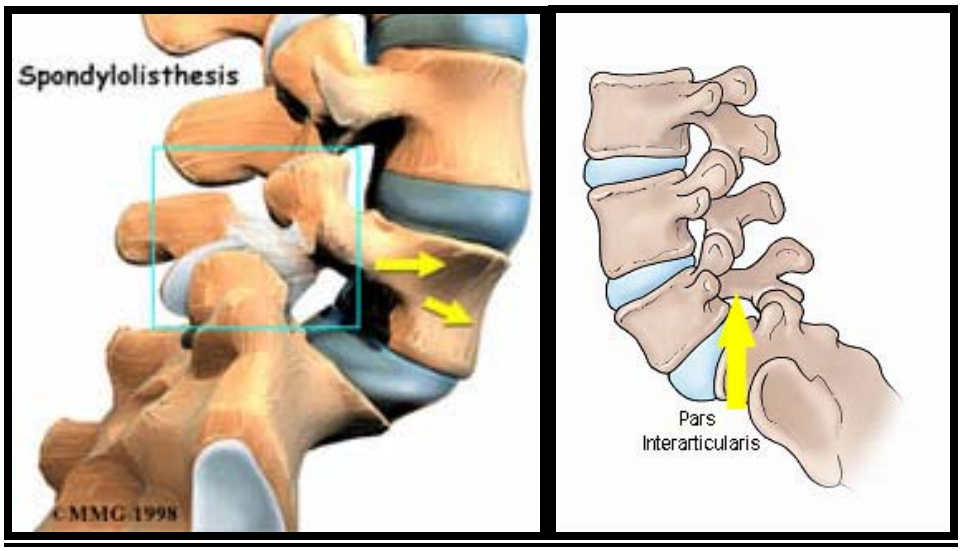

Figure 2-2. Diagram showing the forward slippage of a vertebra relative to the subjacent vertebrae (Left) A defect in the pars interarticularis can cause spondylolisthesis (Right) http://orthoinfo.aaos.org/ and http://www.spine.org/articles/spondylolisthesis.cfm

Spondylolisthesis may not cause any symptoms for years after the slippage has occurred, but the symptoms include low back and buttocks pain, numbness, muscle tightness or weakness in the leg, increased sway back, or a limp. Symptoms usually come from spinal nerves which may be pinched as the vertebrae slips forward. Once symptoms begin, patients usually have constant low grade back discomfort that is aggravated by standing, walking and other activities, while rest will provide temporary relief (North American Spine Society, 2000). The degenerative patient also had irregular bone growth (osteophytes) and fusion of L5 and S1 (Figure 2-3).

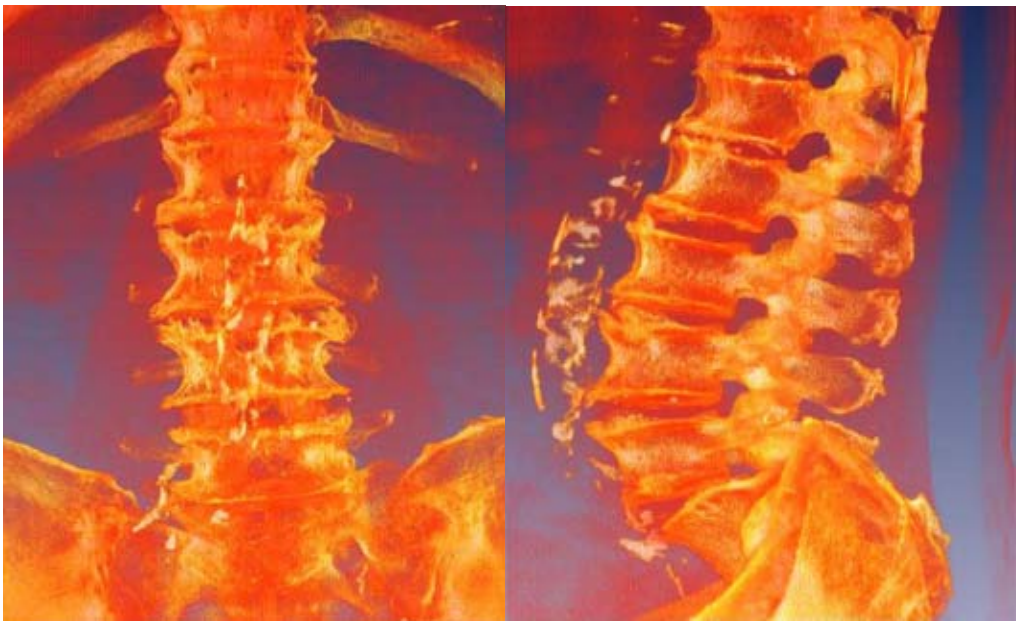

Figure 2-3. Frontal view (Left) and sagittal view (Right) of the degenerative patient.

2.3 Fluoroscopy

The subjects were given informed consent to participate in the study (IRB #0607). Prior to the fluoroscopic evaluation using a VF-2000 fluoroscope (Radiographic and Data Solutions, Inc., Minneapolis, MN), the patients were asked to read and sign a consent form for research. Both subjects underwent fluoroscopic surveillance while performing an active extension / flexion activity. The subjects were asked to start in hyperextension and then perform the activity through full flexion. Single-plane fluoroscopy was used to allow free motion and to allow the activity to be performed in a natural manner. The activity was recorded in the sagittal plane (Figure 2-4). The patient was positioned between the x-ray source and the image intensifier, and was asked to stand as close to the image intensifier as possible (Figure 2-5). The examination allowed for full imaging of L1 to L5 in both patients. The fluoroscopy was conducted using a high frequency, pulsed

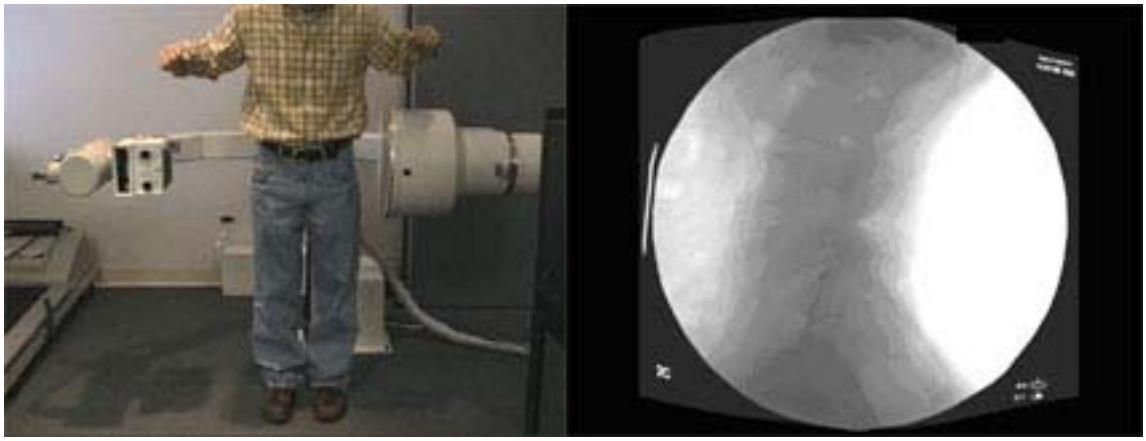

Figure 2-4. Patient undergoing fluoroscopic surveillance while performing extension/flexion (Left) Captured image from the fluoroscopy video (Right).

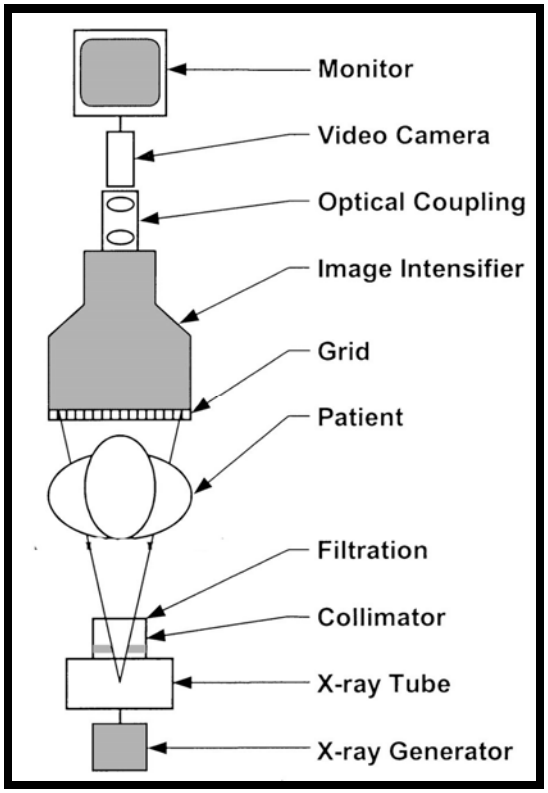

Figure 2-5. Setup of a typical fluoroscopy machine.

unit that records to a computer at a rate of 30 Hz. The radiation exposure of the patient was kept to a minimum due to the pulsed nature of the fluoroscopy. The subjects were subjected to 60 kV and 15 mA with 30 Hz pulses (pulses were 0.003 seconds in duration) for less than 1.5 minutes. The exposure for a patient averages between 1.8 and 3.6 rem for the activity.

Fluoroscopy is advantageous to other methods in that it allows for *in-vivo* analysis under dynamic, weight-bearing conditions. In fluoroscopy, X-rays are emitted from a tube, pass through the patient and strike a fluorescent screen where the images are intensified and recorded on digital video (Figure 2-5). The fluoroscopic process creates a

prospective projection (Figure 2-6). This prospective projection allows for direct observation and analysis of the patient's vertebrae. In this study the bones of the patient's lumbar spine appeared darker than the surrounding soft tissues due to differences in density.

In the perspective projection model, the fluoroscope sensor consists of an X-ray point source and the phosphor screen where the image is formed. The perspective projection was important because 3D motions would not be able to be obtained from the 2D images without it. Accurate geometric models of the vertebrae must be obtained from CT scans as well as an accurate model of the imaging sensor used to form the image. The motion of the vertebrae throughout the activity includes rotations and translations within the plane of the image and out of the plane of the image. After calibration of the fluoroscopy machine and removal of distortion from the images was completed, the focal

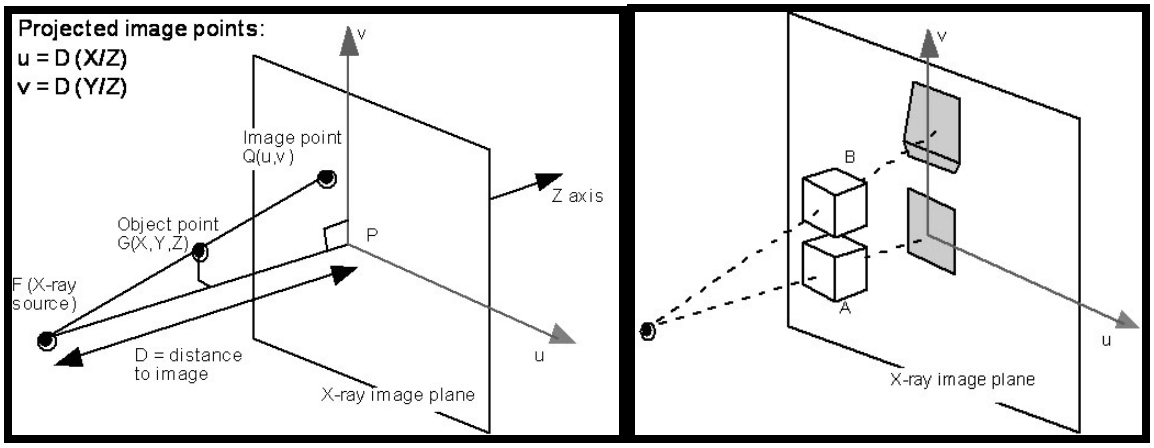

Figure 2-6. Perspective projection imaging model (Left), the silhouettes of the models can be predicted and compared to the observed silhouettes in the image (Right).

length of the imaging system can be determined. This allowed for the out of plane distances to be determined accurately. When the models of the vertebrae and the model of the imaging sensor are known in this perspective projection, it is possible to determine the motions in all six directions: three translational and three rotational.

Individual frames from the fluoroscopic videos were captured on digital video during the performance of the activity at hyperextension, 33% completion of activity, 66% completion of activity, and maximum flexion (Figure 2-7). Images were chosen that were the clearest and easiest to see all of the vertebrae. When an image was encountered that did not have all five vertebrae of interest that were clearly visible, a different image was chosen from the previous or following frames from the video.

The solid, 3D models of the vertebrae were placed over the silhouettes of the corresponding vertebrae in the fluoroscopic images using a computer algorithm based on simulating annealing then manipulates the position of the solid model to minimize an error score which is compromised of edge and area error score. This method will be explained in a later section.

2.4 Image Processing

Still images were captured from the fluoroscopy video at various points to represent the full range of motion for the activity. This was done using Adobe Premiere Pro™ video editing software. The four images captured were at full extension, 33% completion of motion, 66% completion, and at full flexion (Figure 2-7). These images were 640x480 pixels and 8 bits.

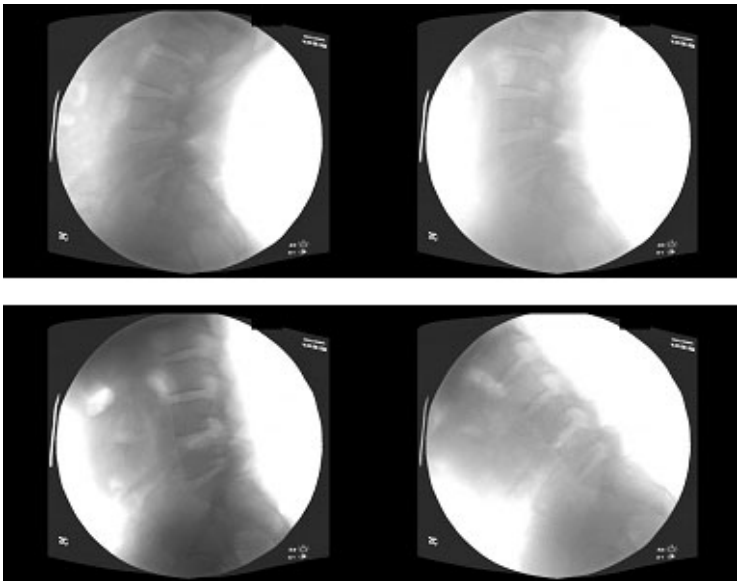

Figure 2-7. Images captured through the entire range of motion.

Before any kinematic data was collected, the distortion associated with the x-ray images had to be corrected. Pincushion distortion and spiral distortion were both encountered with the fluoroscopic images. Pincushion distortion is an outward displacement of an image point from its true location. This type of distortion can be seen in magnification around the outer edge of the image and it occurs when the mapped electrons are transferred from the curved fluorescent image intensifier to the flat output screen. The effect of the pincushion distortion is dependent on the distance from the x-ray source to the image intensifier.

Spiral distortion is caused by electrons being affected by the magnetic field around the image intensifier. This distortion causes rotation and translation of the image. The velocity of the electrons decreases as they approach the output screen while the

magnetic shielding effectiveness increases along the longitudinal axis of the image intensifier. This causes S-shaped distortion in the resulting image.

The 2D spatial transform for each region bounded by four beads is estimated using a known grid of beads. Metal spheres are placed a known distance apart and embedded in plastic. This grid is imaged using fluoroscopy and is used for calibration (Figure 2-8). The dots in the known grid are control points that are compared to the pixel locations of the same dots as seen in the distorted fluoroscopy image. A list of points is created that relate the distorted points to the control points. Transformation coefficients are determined and a function is created to remap the pixels into a reconstructed image. The gray level value of the pixels in the reconstructed image is found using bilinear interpolation between the surrounding pixels in the distorted image (Mahfouz, et al., 2003). These transformation functions were used to remove the distortion from or "unwarp" all the fluoroscopy images before kinematics were determined. After the distortion is removed, the focal length can be computed by a two-plane calibration grid, with a known displacement between plates (Banks et al., 1996; Mahfouz, et al., 2003).

2.5 CT and 3D Model Creation

The normal and degenerative patients were CT scanned using a 16 slice scanner with a slice interval of 0.3 mm. The CT scans of each patient were used to create 3-D models of the L1-L5 vertebrae. Segmentation of the CT slices was done using advanced, commercially available 3D visualization and volume modeling software (AMIRA).

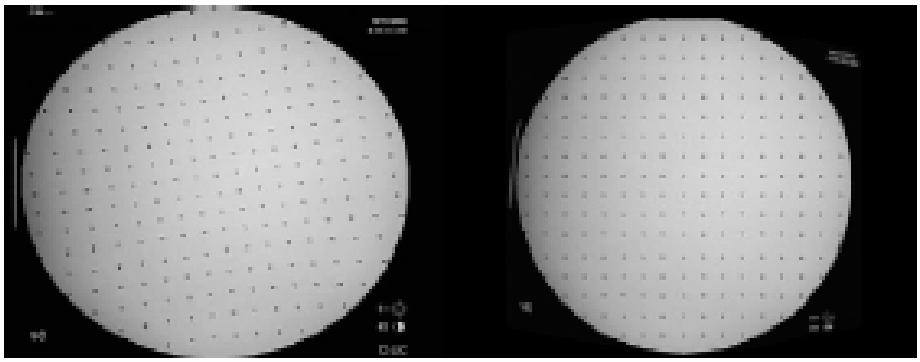

Figure 2-8. Image of beads showing the distortion (Left) and unwarped image of the beads after distortion removal (Right).

Differences in the density between bone and soft tissue were utilized to segment the vertebrae. A threshold value was used to differentiate between density values of bones and muscles in order to remove soft tissue while retaining the bone (Figure 2-9). The slices were reconstructed into 3D models after segmentation was completed on all of the slices (Figure 2-10). These models are specific to the vertebrae of each patient (Figures 2-11 and 2-12). These models were converted to Inventor files made for the Open Inventor Toolkit™ (SGI - Mountain view, CA) which is used in the computer 2D to 3D registration process. Models can be made for any patient that has had a CT scan. The patient specific models were needed in order to be able to accurately register the constructed 3D models to the 2D fluoroscopy images.

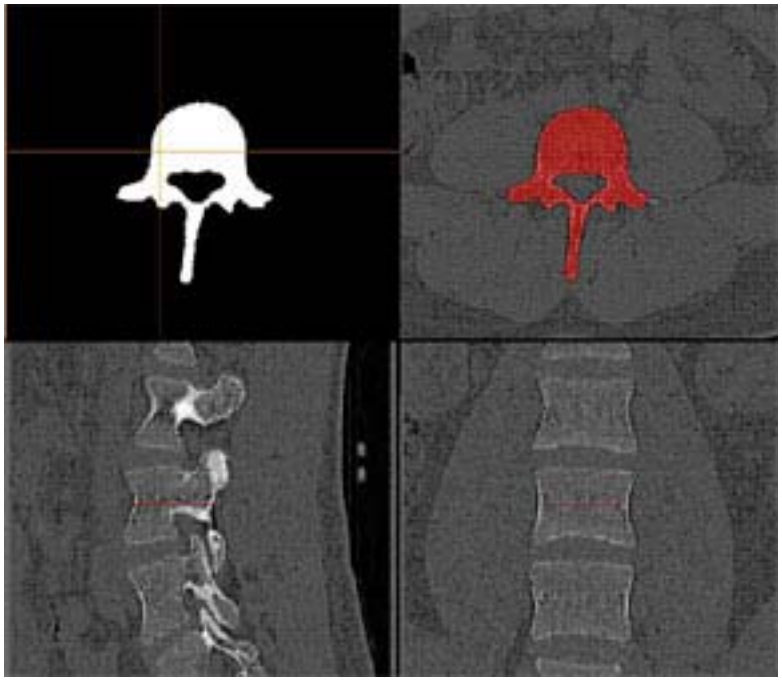

Figure 2-9. Images showing the segmentation process.

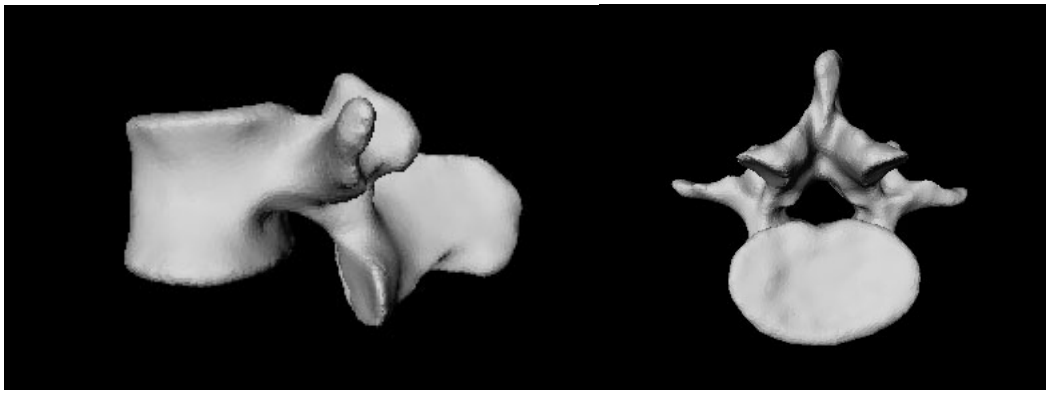

Figure 2-10. Sagittal (Left) and bottom (Right) views of the created 3D vertebral model of the normal patient's L4.

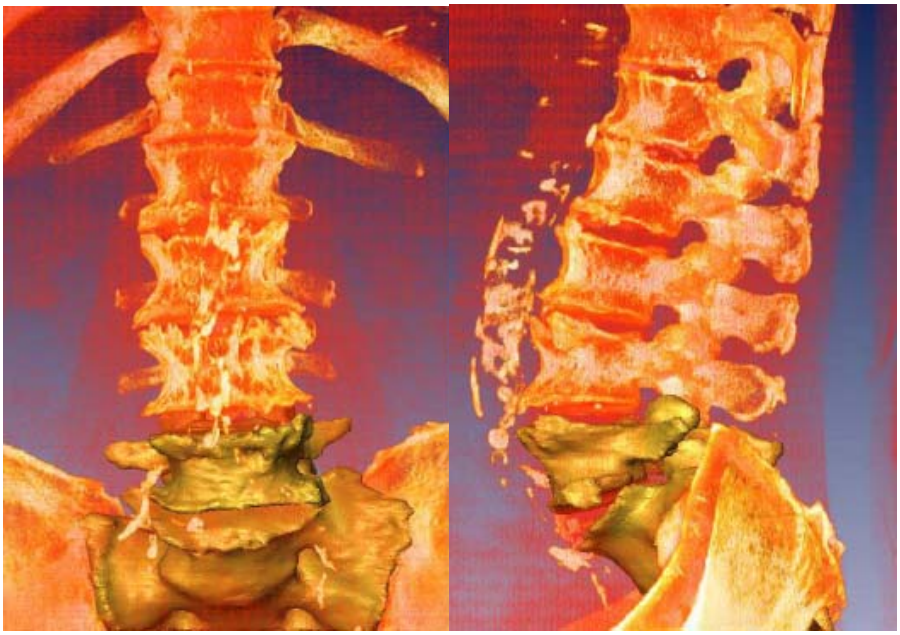

Figure 2-11. Frontal view (Left) and sagittal view (Right) of the L4 and L5 models in the degenerative patient.

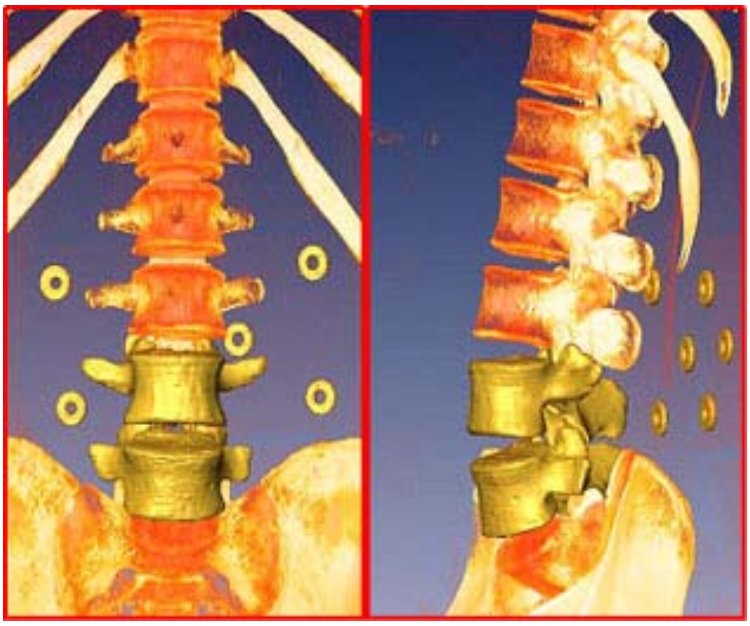

Figure 2-12. Frontal (Left) and Sagittal (Right) views showing the L4 and L5 models for the normal patient.

2.6 2D to 3D Registration

The individual fluoroscopic image frames were analyzed using a software package designed to recreate the three-dimensional position and orientation of the patient's spine from two-dimensional fluoroscopic images. The 2D to 3D registration software creates a virtual scene of the fluoroscopic equipment within the computer. The 3D solid models of the vertebrae can be manipulated until they overlay the silhouettes of the vertebrae in the image. The fluoroscope creates a perspective which can only create one silhouette for a given position and orientation, so recreating this silhouette with the 3D model places that object in the same position and orientations as in the original x-ray image (Figure 2-13). The Open Inventor Toolkit™ (SGI - Mountain view, CA) programming package was used to create a virtual fluoroscope within the computer. The software places the fluoroscopic image in the background of the scene at the location of the image intensifier screen. The vertebral models are placed at the origin of the scene with their centroids aligned so that the models are viewed from the sagittal plane. The goal of the approach used for the 2D to 3D registration was to minimize the error between the recreated prediction of the x-ray pose and the actual pose in the image. The method used included a matching algorithm between the recreated and actual pose and an optimization algorithm. The process was controlled with a graphical user interface which allows for the user to manually fit the initial poses and to control the algorithm.

2.6.1 Matching Algorithm

The image of the predicted pose and the image of the actual pose were compared using a matching algorithm. The 3D models of the vertebrae were white against a black

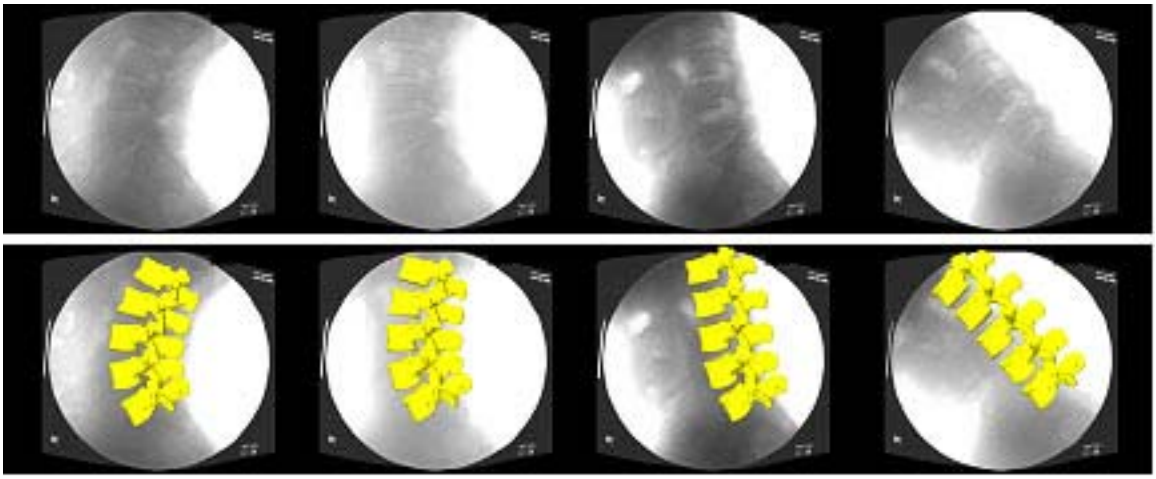

Figure 2-13. Images captured from fluoroscopy (Top) and the3D models registered to the 2D fluoroscopic images (Right).

background in the predicted image. The boundary between the model and the background was found and a growing operation was performed which assigned a contour score to pixels within 3 pixels of the boundary. The contour score was inversely proportional to the distance from the boundary, which allowed the pixels to contribute to the matching score proportionately to their proximity to the boundary. The actual x-ray image was also inverted so that the pixels of the 3D models were white.

The algorithm for evaluating the degree of match between the actual x-ray image and the predicted x-ray image is a combination of an intensity score and a contour score. The matching score between the x-ray image and the predicted pose was found using a weighted combination of metrics. The pixel values of the two images are compared (intensity matching) as well as the overlap of the edges of the images (contour matching). An intensity score is calculated by multiplying the two images together, summing the

result, and normalizing by the area of the model image. Where G(x, y) is the actual x-ray image and H(x, y) is the predicted x-ray image, the intensity matching score is

$$\text{Intensity Matching Score} = \sum_{(x,y)} G(x,y)H(x,y) \; / \; \sum_{(x,y)} H(x,y)$$

The model H is a binary image with nonzero values inside the silhouette. The intensity matching score measures the average gray level intensity of the image G inside the projection of the models. The contour matching score is found in a similar manner as the intensity matching score. Where J(x, y) is the input edge-enhanced image and K(x, y) is the predicted edge image, the contour matching score is

$$\text{Contour Matching Score} = \sum_{(x,y)} J(x,y)K(x,y) \; / \; \sum_{(x,y)} K(x,y)$$

These two scores are combined, with the contour matching value weighted more heavily than the intensity matching value. The intensity matching value helps to guide the 3D vertebral models to the correct pose, but the contour matching value is used to pinpoint the true locations of the models. Since the contour score is more heavily weighted than the intensity value, the contour score dominates when the 3D vertebral models are close to the true solution. The total matching score produces the highest value when the 3D vertebral models are exactly aligned with the silhouettes of the bones in the actual x-ray image. (Mahfouz et al., 2003)

2.6.2 Optimization

A simulated annealing algorithm was used in the optimization step of the 2D to 3D registration. The matching score was recorded at each estimated pose. There could be multiple large minima and smaller local minima in the matching scores. The global minimum was the number of interest because it was the correct solution. A simulated annealing algorithm was chosen to find the global minimum because this algorithm had the ability to get out of local minima. After the user positioned the models initially, a simplex consisting of seven points that represented possible poses and the value of the function space at each point were determined. The algorithm perturbs the worst fit point towards the best fit point and after many iterations there was a convergence to the local minimum.

The optimization technique uses a virtual temperature. The algorithm adds or subtracts a variable that is proportional to the temperature score to the function values of the simplex. The temperature makes some solutions appear better than they are which aids in avoiding local minima. When the temperature score decreases, the likelihood of an increasing error score decreases. The temperature score decreases automatically after a set number of iterations. Local minima can be avoided by lowering the temperature score gradually. The simplex is also expanded periodically to examine the fit of more distant points. The majority of the predicted poses are rejected because they lead to higher matching scores. There are higher scores that occur when the simplex is expanded periodically. The algorithm automatically stops when the difference between the best and worst fit points is less than a small threshold. (Mahfouz et al., 2003)

2.6.3 Error Analysis

Error analysis of the 2-D to 3-D registration system performed on knee model registration found translational error to be less than 0.1 mm in plane (XY plane) and less than 1.4 mm out of plane (Z direction) and rotational error to be 0.4 degrees under ideal conditions (Mahfouz et al., 2003). To determine the error, implants were manually placed in known positions in front of the fluoroscopy machine. Then the image capturing and 2D to 3D registration was performed and compared to the known values. Cadaver legs with implanted knees were monitored by an optotrack system as well as the fluoroscopy machine to compare the results.

The automatic registration could not be used in every case. The user fit was sometimes the only way to get an accurate fit in some images that were occluded and that did not have clear images within a few frames of video. The instances when the automatic registration failed to locate the global minimum were easy to pinpoint because the overlay of the models were obviously not fit to the silhouettes of the vertebrae in the image or the poses or the poses were not likely to occur biomechanically.

2.7 Kinematic Equations

The equations representing the motion of the vertebrae throughout the range of motion were the input into the math model. The three translation and three rotation values of subsequent vertebral bodies with respect to each other and the Newtonian reference frame were obtained from the poses of the vertebrae from the 2D to 3D registration process at each captured position. The transformation matrices of the superior vertebrae relative to the subjacent vertebrae were obtained from the registration.

The kinematic data of transformations and rotations throughout the range of motion was plotted with respect to time (Figures 2-14 and 2-15). These plots were curve-fit and temporal equations were developed for x, y, and z rotation and x, y, and z translation for L4 with respect to (wrt) L5, L3 wrt L4, L2 wrt L3, and L1 wrt L2. These equations were input into the mathematical model as the orientation angles between the vertebrae and the translations between the mass centers of the vertebrae.

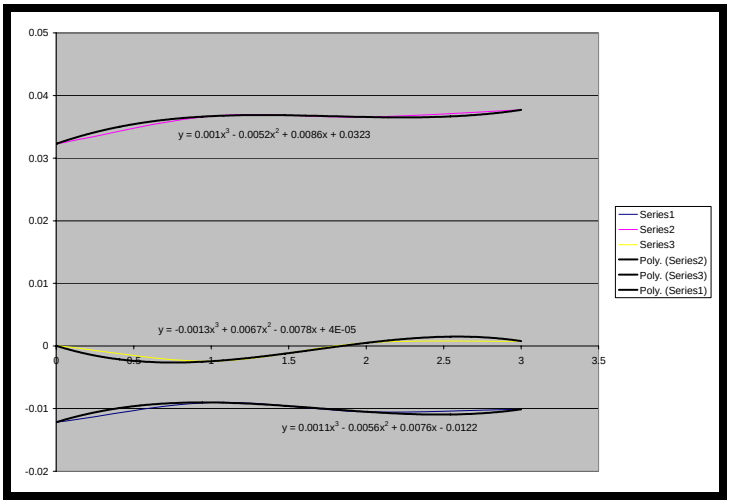

Figure 2-14. Example of curve-fit translation data in all three directions between L1 and L2 in the degenerative patient.

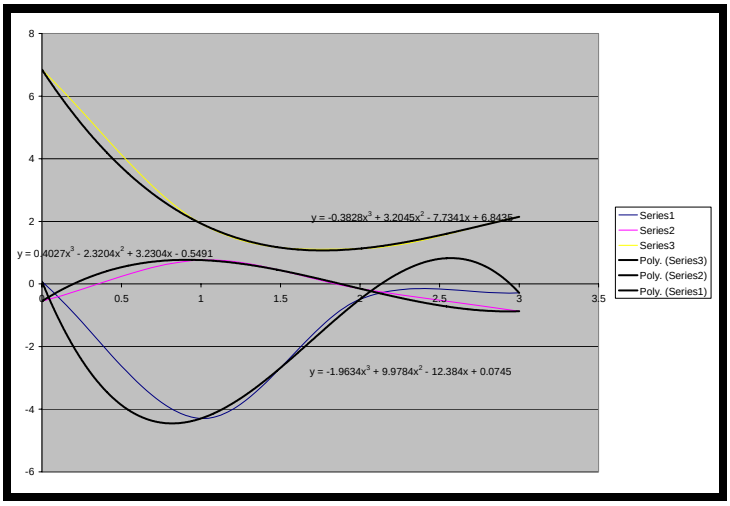

Figure 2-15. Example of curve-fit rotation data in all three directions between L1 and L2 in the degenerative patient.

2.8 Kane's Dynamics

The mathematical model created in this thesis was derived using an inverse dynamics approach. The external load on the system and the motions of the bodies were known inputs into the model. The model had zero degrees of freedom because all motions were specified as inputs using the equations obtained from the registration process and curve-fitting techniques. The purpose of the model is to determine the internal forces in the system which are the interactive forces at the contact point between vertebrae and the resultant body torques. Kane's method of rigid body dynamics was used along with Autolev™ (a computerized symbol manipulation program). Autolev™ is exceptionally fast at simulating multi-body motions, provides automatic simplification of symbolic and numeric expressions, is designed to deal with kinematics, dynamics, statics, energy, mass, and inertia problems, and writes compact C or Fortran programs.

Kane's method was used rather than classical methods such as Newtonian and LaGrangian methods because it focuses on associated motions over configurations (Kane, 1983 and 1985). Kane's method of dynamics allows for the creation and solution of the equations of motion for all of the bodies in a system, simultaneously. Kane's method generates partial velocities and partial angular velocities that lead to generalized forces. Kane's method uses vector methods to determine these velocities and accelerations instead of calculus so problems in differentiation do not arise. Kane's method eliminates non-contributing forces in the system through the use of generalized forces without the incorporation of energy as in Lagrangian methods. This makes Kane's method more efficient than other methods for multibody systems due to the greater simplicity in computation. Newtonian and Lagrangian methods encounter difficulties with the introduction of non-working constraint forces between bodies, the difficulty in the calculation of derivatives, the geometry of the system, and the solution of the governing equations after they are developed (Huston, 1990).

2.8.1 Partial Velocities

Generalized coordinates are scalar variables that describe position vectors of all points and rigid bodies in the system. Generalized speeds are velocity vectors that are functions of the derivatives of the generalized speeds. Generalized speeds describe the speed of a particle or body in respect to a coordinate system. Partial angular velocities and partial velocities are time varying linear functions of generalized speeds.

Auxiliary generalized speeds were introduced into the model to extract the interactive forces and torques that would generally be noncontributing forces in the

system because they make no contributions to the generalized active forces. The auxiliary generalized speeds attribute certain angular velocities and velocities to points that do not correspond to the actual velocities without introducing new generalized coordinates. The generalized speeds cause the partial velocities at the point of application of the force or the partial accelerations of the body on which a torque acts to have non-zero values for certain dot products of partial velocities and partial accelerations.

2.8.2 Equations of Motion

Kane's method of rigid body dynamics develops equations of motion by using the expression:

$$F_r + F_r^* = 0, \quad r = 1, 2, \ldots n$$

Where F_r represents generalized active forces and F_r^* represents the generalized inertia forces

This states that the sum of the generalized active forces and the generalized inertial forces are equal to zero. The generalized active forces are quantities formed by taking dot products of partial velocities and active forces and dot products of partial angular velocities and active torques. The active forces are external contact forces and distance forces such as gravity. The equation for the generalized active forces is:

$$Fr = \sum_{u=1}^{N} [{}^{A}\underline{\mathbf{V}}^{Pi} \cdot \underline{\mathbf{F}}^{i} + {}^{A}\underline{\boldsymbol{\omega}}^{Bi} \cdot \underline{\mathbf{T}}^{Bi}]$$

Where ${}^{A}\underline{\mathbf{V}}^{Pi}$ represents the partial velocities of the rigid bodies

$\underline{\mathbf{F}}^{i}$ represents the resultant active forces

${}^{A}\underline{\boldsymbol{\omega}}^{Bi}$ represents the partial angular velocities of the rigid bodies

$\underline{\mathbf{T}}^{Bi}$ represents the resultant active torques

The generalized inertia forces are quantities formed by taking dot products of partial velocities and inertia forces and dot products of partial angular velocities and inertia torques. The inertia forces are forces due to the mass of a body. The equation for the generalized inertia forces is:

$$Fr^{*} = \sum_{u=1}^{N} \left[{}^{A}\underline{\mathbf{V}}^{Pi} \cdot \underline{\mathbf{F}}^{i*} + {}^{A}\underline{\boldsymbol{\omega}}^{Bi} \cdot \underline{\mathbf{T}}^{Bi*} \right]$$

Where ${}^{A}\underline{\mathbf{V}}^{Pi}$ represents the partial velocities of the rigid bodies

$\underline{\mathbf{F}}^{i*}$ represents the resultant inertia forces

${}^{A}\underline{\boldsymbol{\omega}}^{Pi}$ represents the partial angular velocities of the rigid bodies

$\underline{\mathbf{T}}^{i*}$ represents the resultant inertia torques

$$\underline{\mathbf{F}}^{i*} = -m_{Pi}\,(\underline{\mathbf{a}}^{Pi}) \qquad \text{and} \qquad \underline{\mathbf{T}}^{Bi*} = -\underline{\boldsymbol{\alpha}}^{Bi} \cdot I - \underline{\boldsymbol{\omega}}^{Bi} \times (I \cdot \underline{\boldsymbol{\omega}}^{Bi})$$

Where m_{Pi} is the mass of Pi

$\underline{\mathbf{a}}^{Pi}$ is the acceleration of Pi

$\underline{\boldsymbol{\alpha}}$ is the angular acceleration of a body in another reference frame

I is the central inertia dyadic of the body

$\underline{\boldsymbol{\omega}}$ is the angular velocity of the body in another reference frame

Once all generalized active forces and generalized inertia forces are known, the equations of motion can be formulated by using the Autolev™ command $Fr + Fr^{*}=0$. This equation states that the sum of the active forces and the passive forces in the system is equal to zero. The number of equations created is equal to the number or generalized speeds. Each generalized speed is introduced to solve for an unknown, so the number of generalized speeds equals the number of unknowns.

2.9 Mathematical Model

2.9.1 Assumptions

There were several assumptions made in the creation of the model (see FBD Figure 2-16). The first assumption is that the weight of the upper body (everything above L1) is the input force into the system. This weight was taken to be 0.4 * the patient's body weight (Winter, 1990). Another assumption that was made is that the L5 vertebra was fixed. There were no muscle forces included in the model for simplification purposes. The muscle forces are evident within the torques between bodies.

2.9.2 Theory

A free body diagram (FBD) of the system was developed (Figure 2-16). A Newtonian reference frame was created as an inertial reference frame. The command AUTOZ ON was used to allow Autolev™ to automatically replace expressions with symbols allowing for more efficient evaluation of direction cosine matrices. The bodies A, B, C, D, and E were introduced using the BODIES command to represent the five

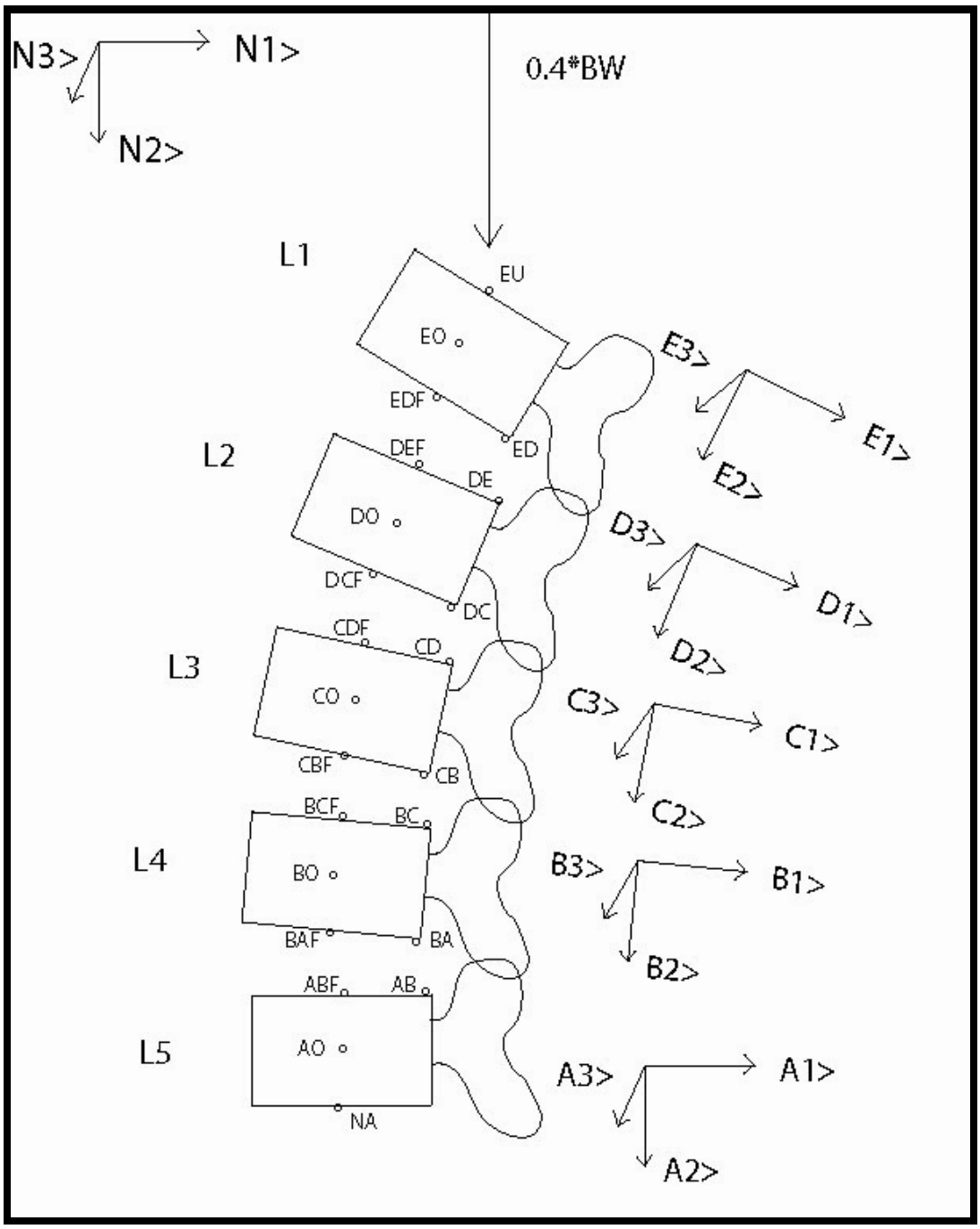

Figure 2-16. Free body diagram used to construct the mathematical model.

lumbar vertebrae: body A represented L5, body B represented L4, body C represented L3, body D represented L2, and body E represented L1. The BODIES command declares names of rigid bodies and defines the mass center of the body. The FRAMES command was used to create a reference frame with a set of mutually perpendicular unit vectors fixed in that frame. Frames were introduced in order to perform the simple rotations of one vertebra relative to another vertebra. Next, the POINTS command introduced the various points on the rigid bodies used to determine the unit vectors that describe the reference frame for each body (see FBD, Figure 2-16). Constants for gravity and the body weight of the patient were defined. The masses of the bodies were defined and the direction of gravity was specified. An external load of 0.4*BW was applied on the system to represent the weight of the upper body above L1.

Generalized speeds, their time derivatives and the variables that were solved for were introduced using the VARIABLES command. Twenty four generalized speeds were introduced to allow for extraction of the unknown forces and torques that would not show up in the equations of motion without the introduction of the generalized speeds because they do not contribute to the generalized active forces. The variables that were solved for were interactive forces in three directions between each vertebral level: L4-L5, L3-L4, L2-L3, L1-L2, and torques in three directions of each body relative to the subjacent body: L4 on L5, L3 on L4, L2 on L3, and L1 on L2 (Figure 2-17). It is imperative when modeling a system, especially the human body, that a moment and a torque are not the same. All torques are moments, but not all moments are torques. Therefore, we modeled the lumbar spine understanding the differences between torques and moments. Since muscles were not modeled specifically, we assume that at each

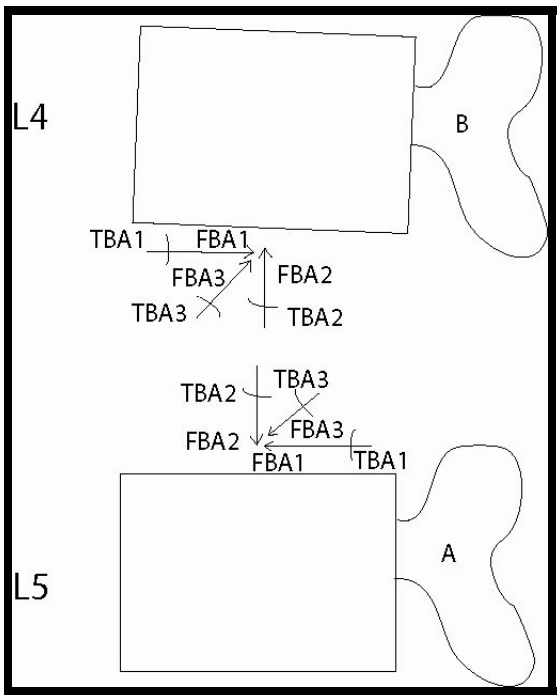

Figure 2-17. Example of forces and torques solved for at the L4 - L5 level.

vertebral interface, a resultant torque encompassed all of the muscles across the joint. These torques can be thought of as motors causing rotation to occur.

The Euler or orientation angles of the system were specified using the curve-fit temporal equations obtained from the rotations between the vertebrae. The L5 vertebral body was set as a fixed body, so the angles between the Newtonian frame and the frame for body A were zero around all three axes. ΘNA1, ΘNA2, and ΘNA3 are the rotations between L5 and the Newtonian frame around the three axes, which are all zero since L5 is fixed in the model. ΘBA1, ΘBA2, and ΘBA3 are the rotations between L4 and L5, ΘCB1, ΘBC2, and ΘBC3 are the rotations between L3 and L4, ΘDC1, ΘDC2, and

ΘDC3 are the rotations between L2 and L3, and ΘED1, ΘED2, and ΘED3 are the rotations between L1 and L2.

The sequential rotations of the system were performed using the SIMPROT command. The order of rotations that was used was a fixed Newtonian x, y, z order (N1>, N2>, N3>) (Figure 2-18). The SIMPROT command relates mutually perpendicular vectors fixed in one frame to mutually perpendicular vectors fixed in another frame. The SIMPROT command formed the direction cosine matrix associated with a simple rotation of one frame relative to another frame. To perform this rotation a vector whose orientation in both frames does not change during the rotation is needed as well as the angle of the rotation. Three simple rotations were done for each vertebra relative to the subjacent vertebrae.

The ANGVEL command expresses the angular velocity of the second frame in frame one and is expressed in terms of Euler parameters, their time-derivatives, and mutually perpendicular unit vectors fixed in the second frame. The angular velocities were redefined in order to introduce twelve generalized speeds into the system.

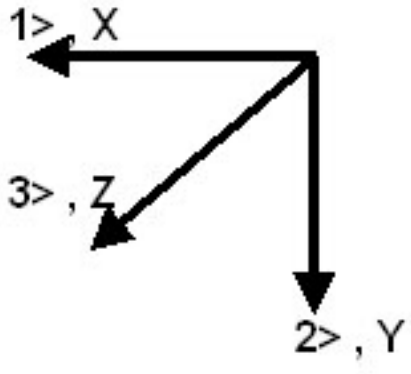

Figure 2-18. Orientation of axes.

The angular velocity of body B in reference frame N ($^{N}\underline{\boldsymbol{\omega}}^{B}$) was previously defined as the angular velocity of body A in reference frame N ($^{N}\underline{\boldsymbol{\omega}}^{A}$) + the angular velocity of body B in reference frame A ($^{A}\underline{\boldsymbol{\omega}}^{B}$). $^{N}\underline{\boldsymbol{\omega}}^{B}$ was redefined as $^{N}\underline{\boldsymbol{\omega}}^{A}$ + $^{A}\underline{\boldsymbol{\omega}}^{B}$ + three generalized speeds. $^{N}\underline{\boldsymbol{\omega}}^{C}$, $^{N}\underline{\boldsymbol{\omega}}^{D}$, and $^{N}\underline{\boldsymbol{\omega}}^{E}$ were defined in the same manner with three generalized speeds introduced for each angular velocity.

The scalar quantities that were used to form the position vectors between the points were input into the model. There were fixed points at the center of the superior and inferior endplates of the vertebrae and at the mass center. The distances between the fixed points were measured using SigmaScan™. There were also variable contact points that were defined by position vectors that went from the fixed point to the contact point as the contact point moved throughout the range of the activity. The variable contact points were also measured using SigmaScan™. The distance from the fixed central point to arbitrarily assigned contact points was measured. The initial contact point was placed at the posterior point of the vertebral body and the final contact point was placed at the anterior point of the vertebral body. The other two contact points were placed equally between these two points. This estimation was an initial model of the contact point that was determined from looking at the fluoroscopic images throughout the range of motion to see where the contact appeared to be occurring. The measured distances were curve fit to give equations for the change in the contact point position over time. The position vectors were formed by assigning directions to the previously defined scalars.

The translations of one vertebral body relative to the subjacent vertebral body were also found from the 2D to 3D registration process in a similar manner as the rotations were found. The temporal equations representing the translations of one

vertebral body relative to the subjacent vertebral body were input into the model. The translations were input into the model as position vectors between the mass centers of the vertebrae.

The partial velocities of each of the defined the points were obtained. The velocities of NA and ANF were both zero because L5 (body A) was fixed to the Newtonian frame. The velocities of the fixed points AO, ABF, BCF, BO, CO, CDF, DO, DEF, EO, and EU were found using the command V2PTS. This command finds the velocity in the first reference frame (A) of a point Q in a second reference frame (B) if the velocity in the first reference frame of another point P in the second reference frame is known (B). The angular velocity of the second reference frame (B) in the first reference frame (A) and the position vector from point (P) to point (Q) must also be known.

V2PTS(A,B,P,Q)

Where,

A=first reference frame

B=second reference frame

P=first point fixed in the second reference frame

Q=second point fixed in the second reference frame

The velocity of AB in reference frame N ($^{N}\underline{\mathbf{V}}^{AB}$) was found by adding the derivative of the position vector from ANF to AB in reference frame N. ($^{N}\underline{\mathbf{V}}^{BA}$) was equal to ($^{N}\underline{\mathbf{V}}^{AB}$), but the velocity was redefined to include three generalized speeds. Nine more generalized speeds were introduced in the velocity equations for $^{N}\underline{\mathbf{V}}^{CB}$, $^{N}\underline{\mathbf{V}}^{DC}$, and $^{N}\underline{\mathbf{V}}^{ED}$

at the contact points. The velocity of BAF in reference frame N ($^{N}\underline{\mathbf{V}}^{BAF}$) was found by adding the derivative of the position vector from BA to BAF in reference frame B to the velocity of BA in reference frame N ($^{N}\underline{\mathbf{V}}^{BA}$). $^{N}\underline{\mathbf{V}}^{CBF}$, $^{N}\underline{\mathbf{V}}^{DCF}$, and $^{N}\underline{\mathbf{V}}^{EDF}$ were found in the same manner as ($^{N}\underline{\mathbf{V}}^{BAF}$).

After the velocities of the points were known, the auxiliary generalized speeds were constrained. Then the expressions for the forces and torques were developed. The external input force was defined as 0.4*BW and was applied at point EU which was the top of the L1 vertebra. The direction of the force was in the y (N2>) direction (Figure 2-17).

Autolev™ creates a set of dynamic, differentiable, algebraic equations in response to the command ZERO = FR () + FRSTAR (). The commands FR and FRSTAR prompt Autolev™ to form expressions for the generalized active forces and generalized inertia forces. The command KANE solves this set of equations for the unknown force and torque values (Figure 2-18). Autolev creates a C code that performs the actual calculations that solves for the unknown values. The desired outputs were defined and were plotted against time or flexion angle.

2.9.3 Sensitivity Analysis

A sensitivity analysis was conducted to determine which parameters within the mathematical model could alter the results most significantly if they were incorrectly modeled or entered as input data.

3 RESULTS

3.1 Kinematic Results

The 3D motions of all of the bodies can be obtained throughout the entire range of the motion using the previously described methods. The ranges of motion in the degenerative and normal patient were significantly different (Figures 3-1 and 3-2). The flexion angle was taken as the angle around the z axis (3 direction) between the L4 and L5 vertebrae. The range of motion around this axis in the degenerative patient was 6.01° and 13.47° in the normal patient. The degenerative and normal patients were facing in different directions while performing the activity which can be seen in Figures 3-1 and 3-2. Since L5 was fixed in the model, the limited range of motion in the degenerative patient as compared to the normal patient could easily be seen in Figures 3-1 and 3-2. The motion for the degenerative patient ranged only 0.969° past vertical where the normal patient flexed 9.25° past vertical. This difference in motion led to differences in the kinetics between the degenerative and normal patient which was evident in the shapes of the force and torque data curves.

The rotation around the z axis (3 axis) at the L3-L4 level in the degenerative patient was larger than at the other levels (Figure 3-3). The motion was similar to the motion at the same level in the normal patient. This increase in range of motion at this level may be compensating for loss of motion in the lower degenerative levels.

The difference in the range of motion around the z axis (3 axis) can be seen in Figures 3-1 and 3-2, but the differences in the motions in other directions could not be seen from these figures. The rotations around the other two axes x (1>) and y (2>) were

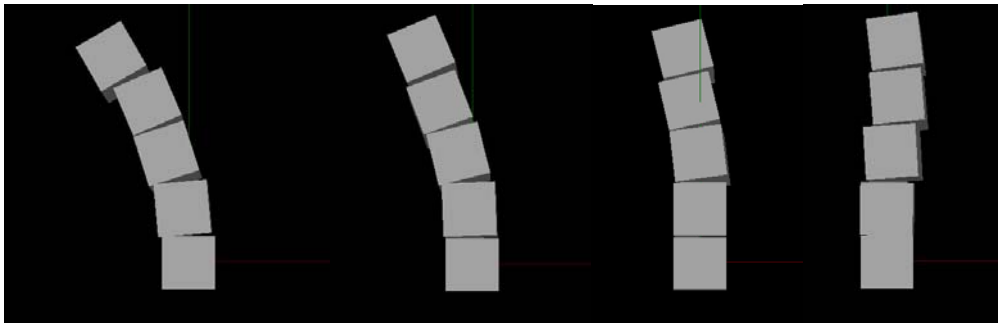

Figure 3-1. Range of motion in the degenerative patient from maximum extension (Left) to maximum flexion (Right).

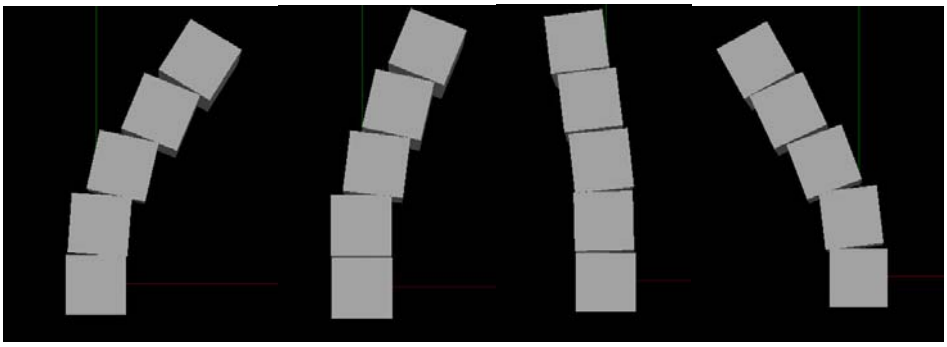

Figure 3-2. Range of motion in the normal patient from maximum extension (Left) to maximum flexion (Right). The patient was facing in the opposite direction as the degenerative patient.

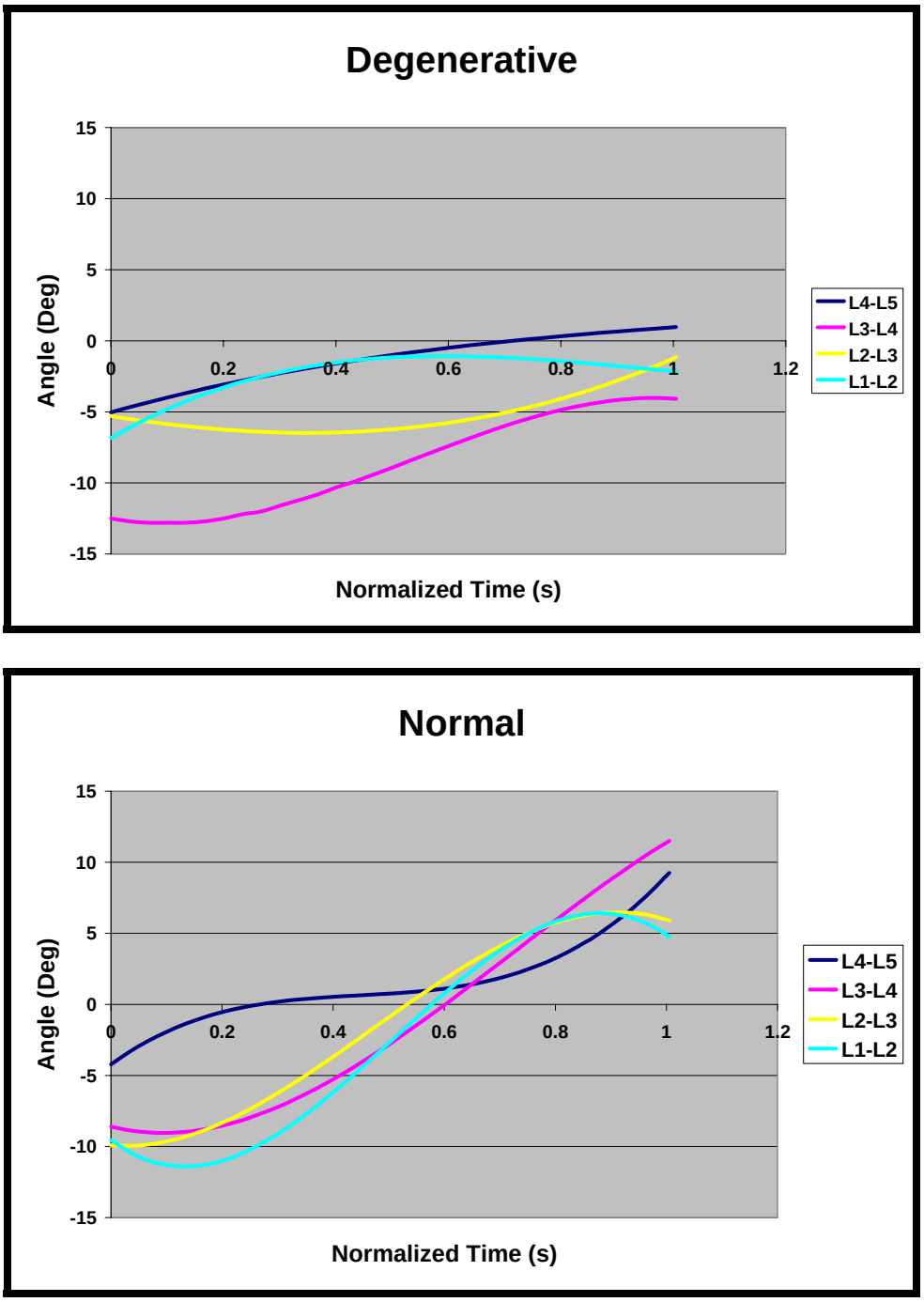

Figure 3-3. Orientation Angles around the z axis (3 direction) in the degenerative patient (Top) and the normal patient (Bottom).

greater in the degenerative patient than in the normal patient (Figures 3-4 and 3-5). The rotations around the x axis in the degenerative patient ranged from 4.5 to -0.75° at L1-L2, 0 to -5° at L2-L3, -2.75 to -8.2° at L3-L4, and 4.0 to -1.0° at L4-L5. The ranges of motion around the x axis in the normal patient were smaller with the range being 0.1 to -2.3° at L1-L2, 0 to -2.5° at L2-L3, 1.3 to 0.3° at L3-L4, and 2.2 to -1.0° at L4-L5.

The rotations around the y axis were also greater in the degenerative patient than in the normal patient. The motion around the y axis in the degenerative patient ranged from 1.0 to -1.0 ° at L1-L2, 4.25 to -0.25° at L2-L3, 2.75 to -6.2° at L3-L4, and 0 to -3.0° at L4-L5. The motion around the y axis in the normal patient ranged from -0.2 to -2.2 at L1-L2, 0 to -1.6° at L2-L3, 1.7 to -0.6° at L3-L4, and 0 to -1.2° at L4-L5.

3.2 Kinetic Results

Twenty four unknowns were solved for using the mathematical model. Twelve interactive contact forces and twelve body torques were calculated. Three forces and torques were found at each vertebral level: L1-L2, L2-L3, L3-L4, and L4-L5. The force and torque results were plotted and normalized with respect to time where maximum extension represented time equal to zero seconds, 33% completion of the activity occurred at 1.0 second, 66% completion of the activity occurred at 2.0 seconds, and full flexion occurred at 3.0 seconds (Appendix B). The results were also plotted against flexion angle. The angle used for the flexion angle was the angle around the z axis (3 direction) between L4 and L5.

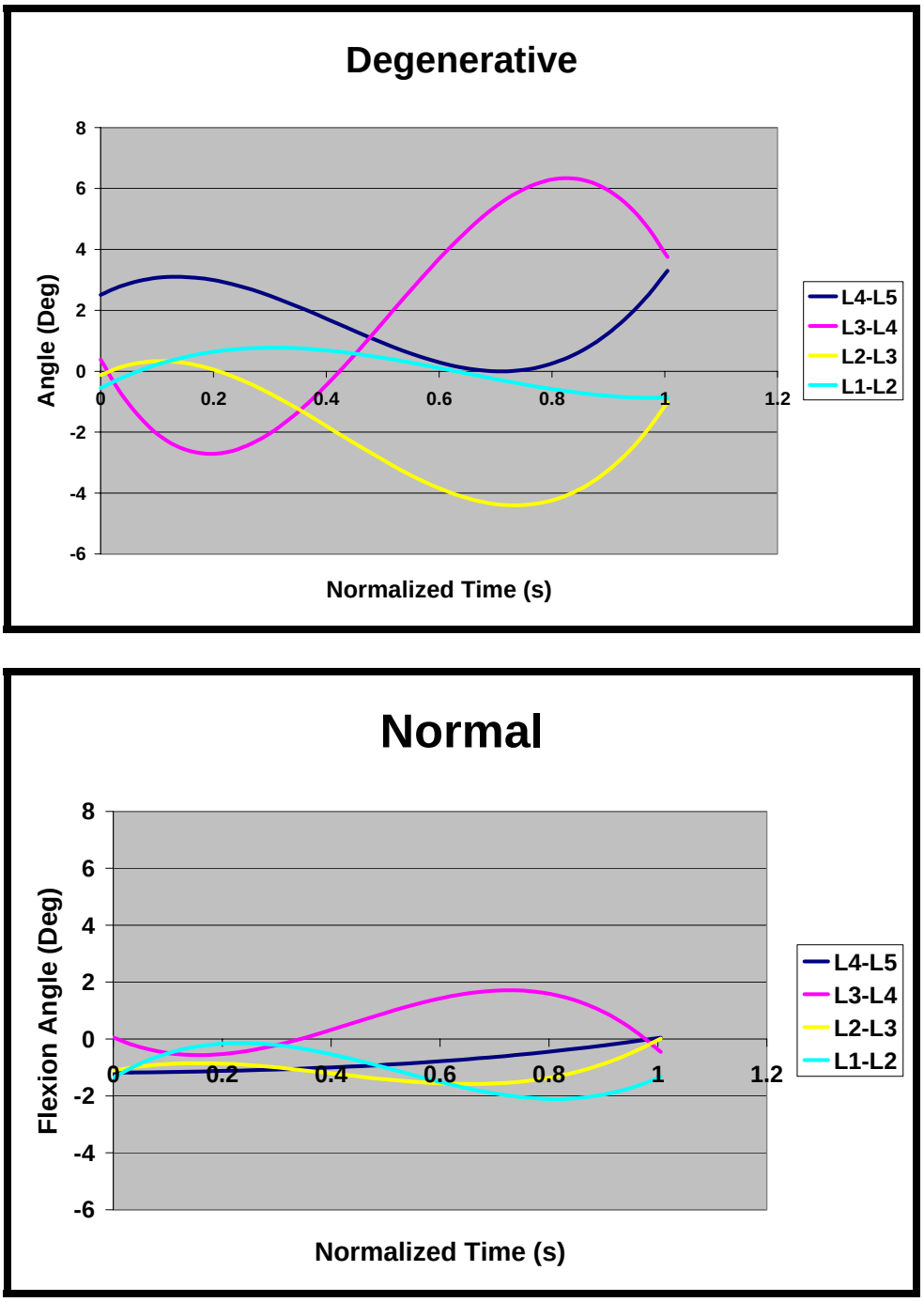

Figure 3-4. Orientation Angles around the y axis (2 direction) in the degenerative patient (Top) and the normal patient (Bottom).

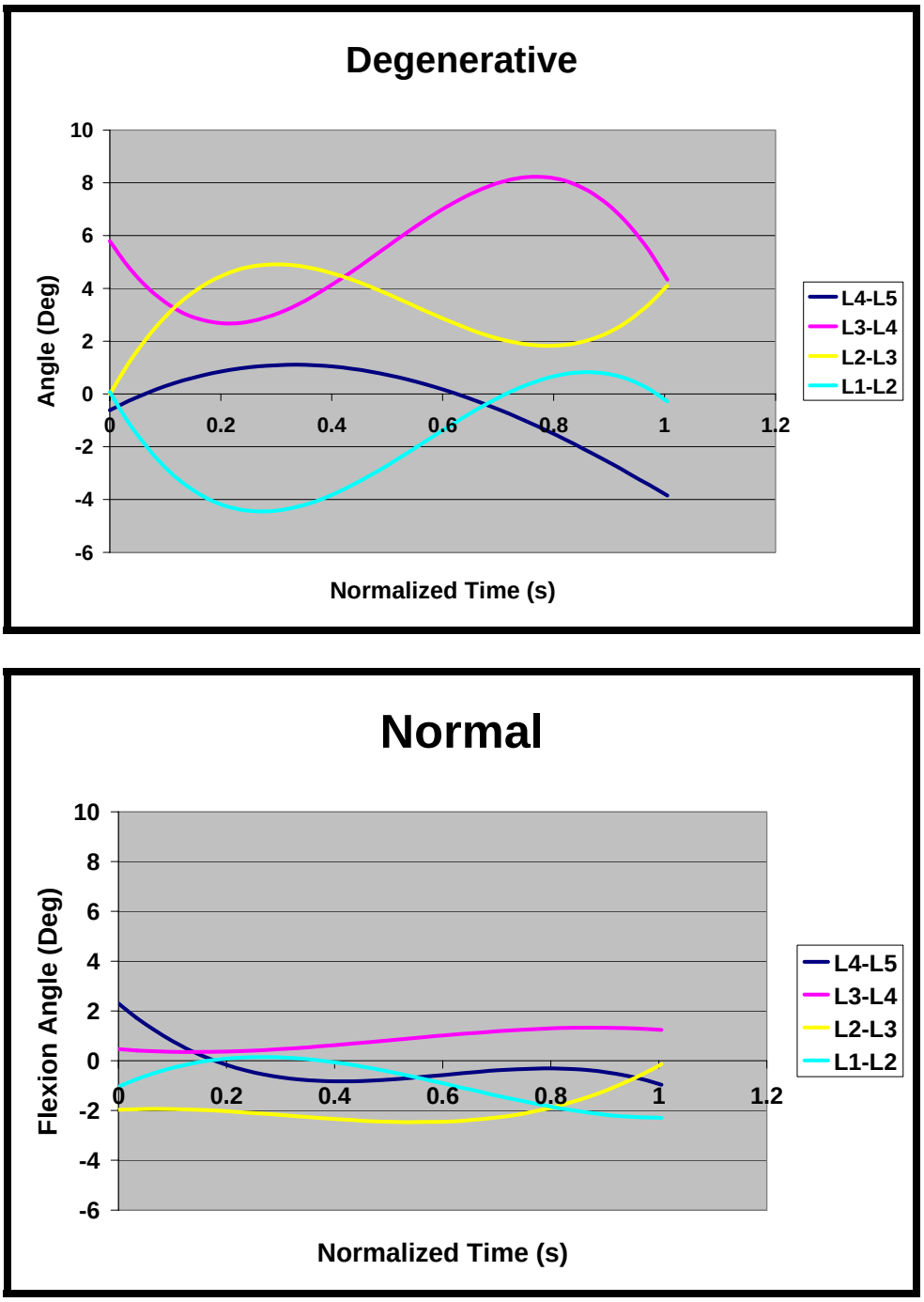

Figure 3-5. Orientation Angles around the x axis (1 direction) in the degenerative patient (Top) and the normal patient (Bottom).

The force results were very similar in the degenerative and the normal patient. The differences between the patients were more evident in the torque results. The forces in the degenerative and normal patient were similar at all levels (Figure 3-6). The resultant forces in the degenerative patient and the normal patient ranged from 0.4 to 0.43 times body weight (Table 1). The maximum vertical force at the L1-L2 level was 0.405 times body weight in both the degenerative and normal patient. The maximum vertical force at the L2-L3 level was 0.41 times body weight in both patients. The maximum vertical force at the L3-L4 level was 0.415 times body weight for both patients. The maximum vertical force at the L4–L5 level was 0.42 times body weight in both the normal and the degenerative patient.

The transverse forces, in the x (1) and z (3) were also calculated in both patients. The transverse forces in the x direction (1 direction) were very similar in both patients (Figure 3-7). The maximum transverse force in the x direction at L1-L2 was 0.2*BW for both patients. The maximum transverse force in the x direction at L2-L3 was 0.15*BW in the normal patient and 0.125 * BW in the degenerative patient. The maximum force in the x direction in the normal patient occurred in full flexion. The force in the x direction

Table 1. Maximum vertical force in both patients.

Level	Vertical Force
L1-L2	0.405*BW
L2-L3	0.41*BW
L3-L4	0.415*BW
L4-L5	0.42*BW

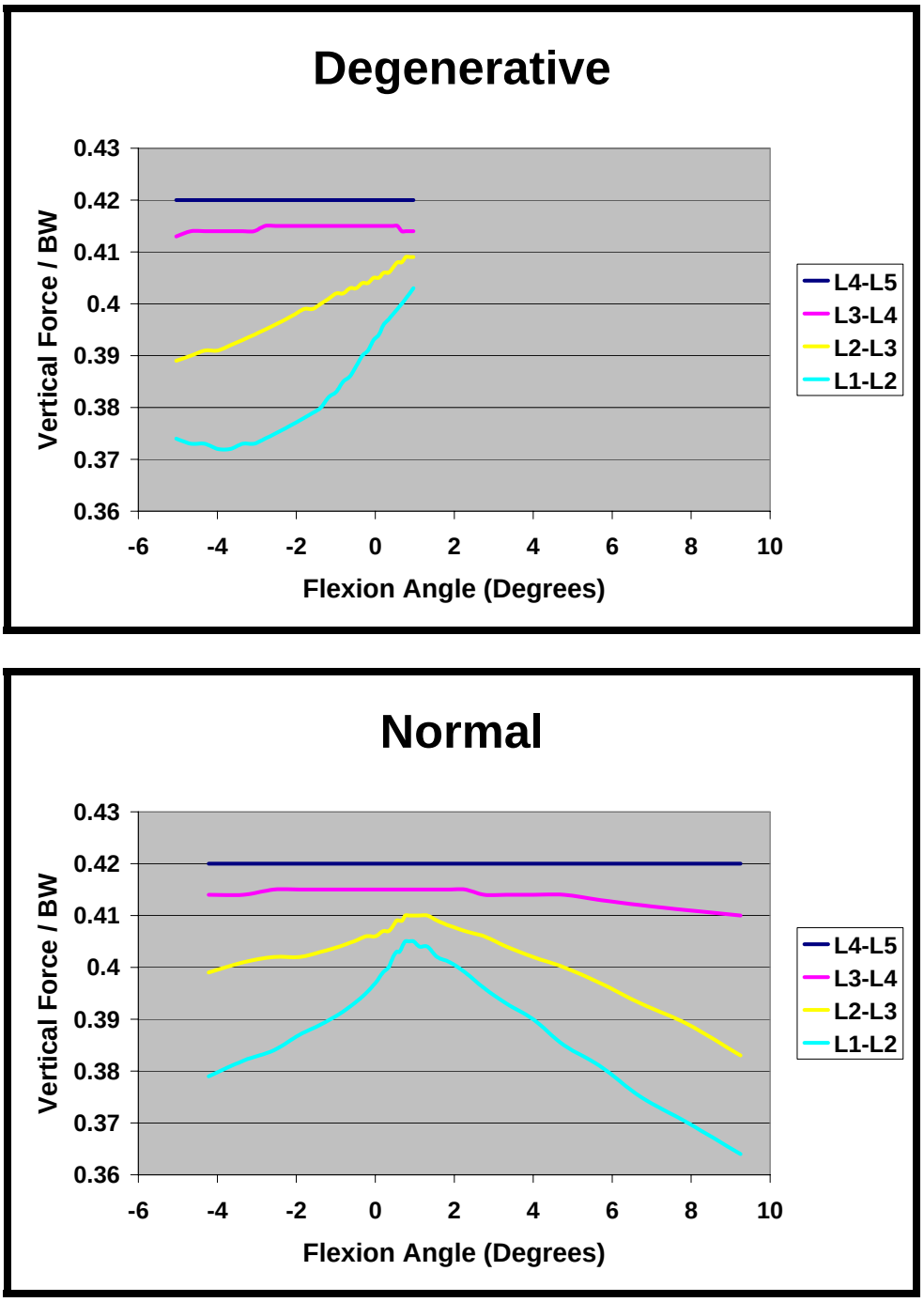

Figure 3-6. Vertical forces at every level for the degenerative patient (Top) and the normal patient (Bottom).

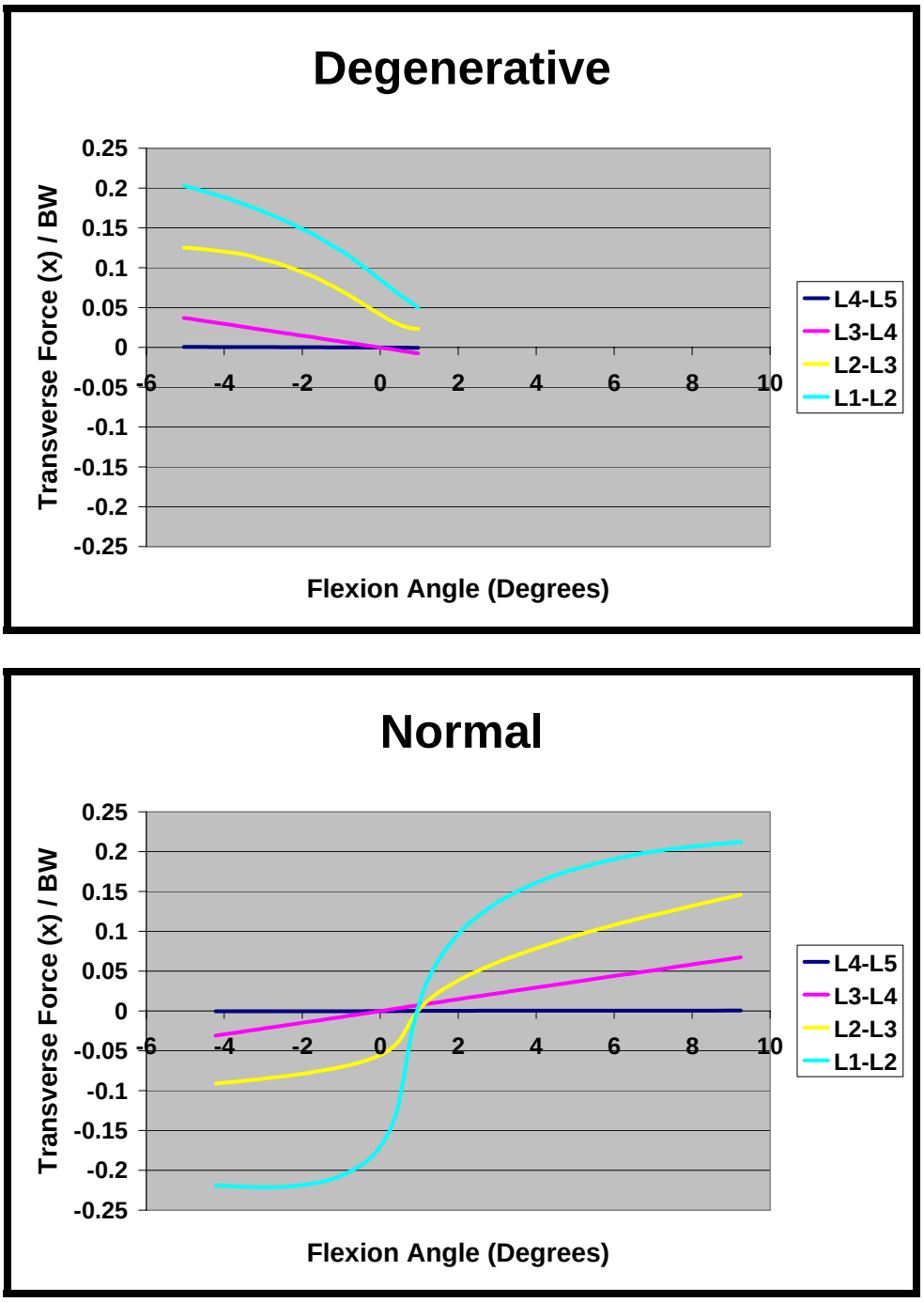

Figure 3-7. Transverse forces in the x (1) direction at every level for the degenerative patient (Top) and the normal patient (Bottom).

at maximum extension was 0.125* BW in the degenerative patient and 0.1*BW in the normal patient. The force in the x direction at maximum extension at the L3-L4 level was 0.04*BW in both patients. The force in the normal patient at maximum flexion was 0.054*BW. The maximum transverse force in the x direction at L4-L5 was close to zero in both patients.

The transverse forces in the z direction (3 direction) were slightly higher in the degenerative patient than in the normal patient (Figure 3-8). The maximum force in the z direction at the L1-L2 level was 0.06*BW in the degenerative patient and 0.0225*BW in the normal patient. The maximum force in the z direction at L2-L3 was 0.05*BW in the degenerative patient and 0.0175*BW in the normal patient. The maximum force in the z direction at L3-L4 was 0.03*BW in the degenerative patient and 0.015*BW in the normal patient. The maximum force in the y direction at the L4-L5 level was close to zero in both cases.

The differences in the kinetics between the degenerative and normal patient were more evident in the calculated torques values than in the force values. The resultant torques and the torques around all three axes were calculated at each level: L4 on L5, L3 on L4, L2 on L3, and L1 on L2 (Figures 3-9 through 3-15).

The torque results for the L1-L2 level can be seen in Figure 3-9. The resultant torque in maximum extension at the L1-L2 level was 4.05 N*m in the degenerative subject and 4.07 N*m in the normal subject (Table 2). The degenerative patient's maximum flexion was only one degree past vertical and the resultant torque was 1.14 N*m at that point. The maximum flexion of the normal patient was over 9° past vertical.

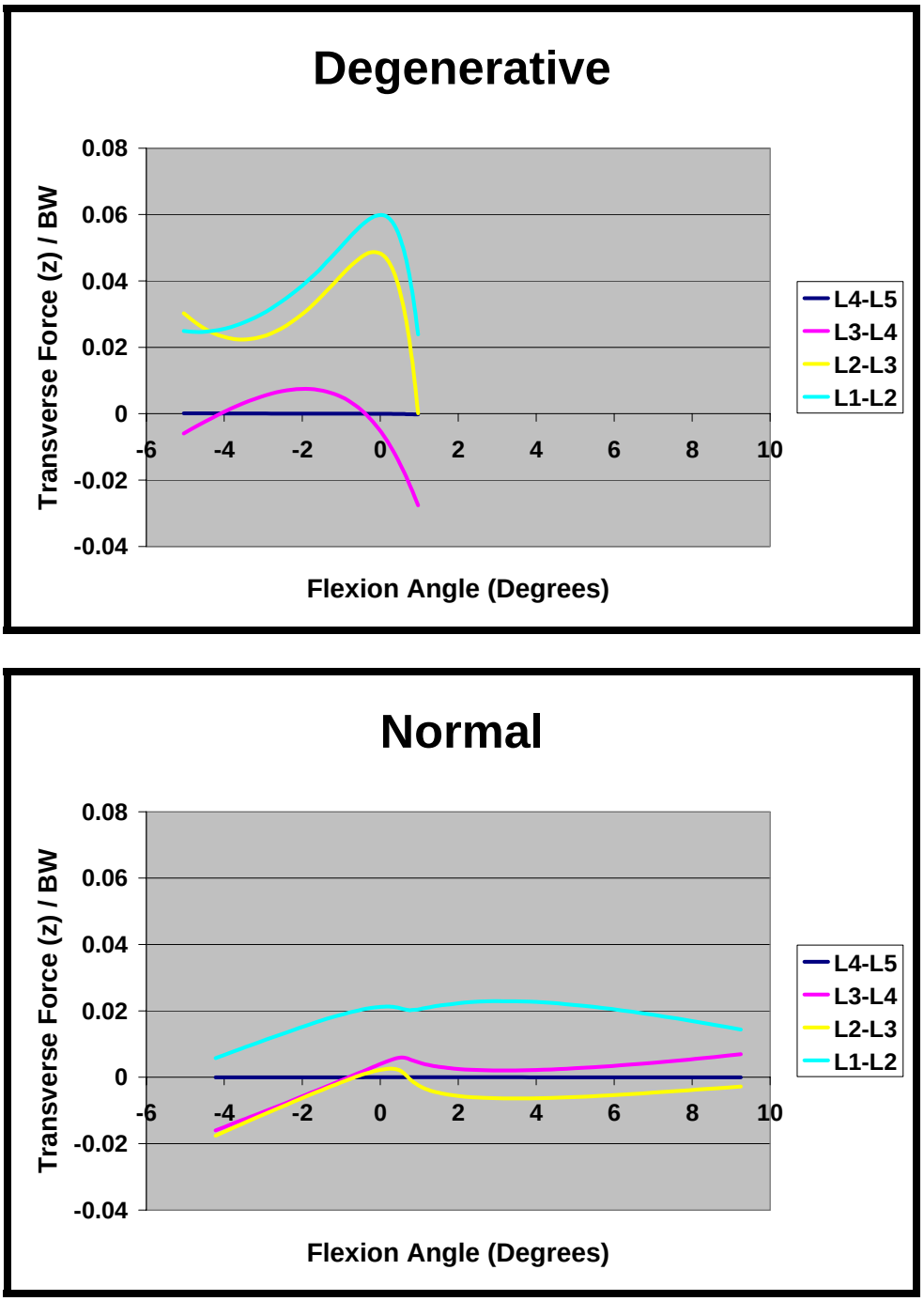

Figure 3-8. Transverse forces in the z (3) direction at every level for the degenerative patient (Top) and the normal patient (Bottom).

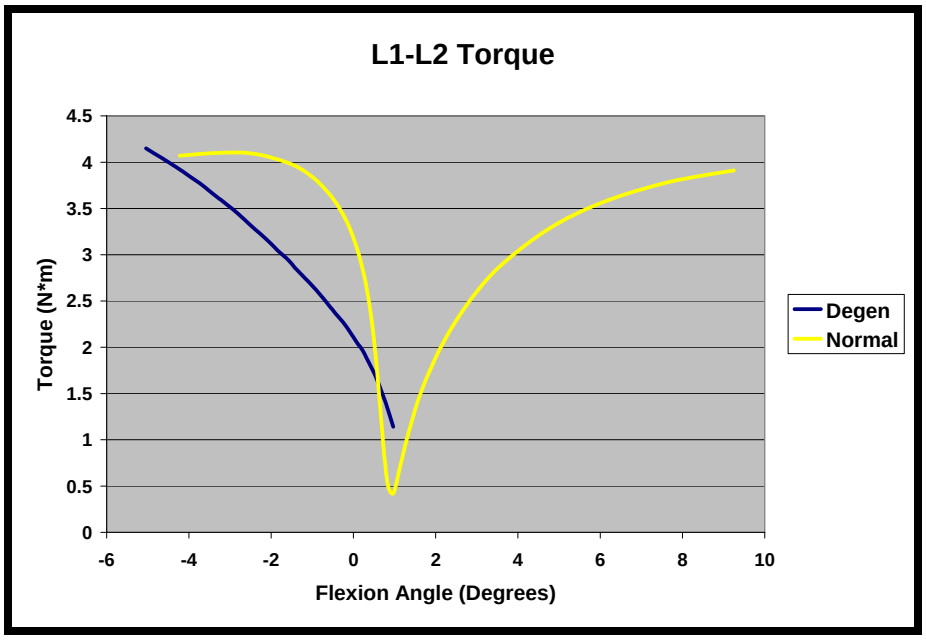

Figure 3-9. Resultant torques between L1 and L2 for the degenerative patient and the normal patient.

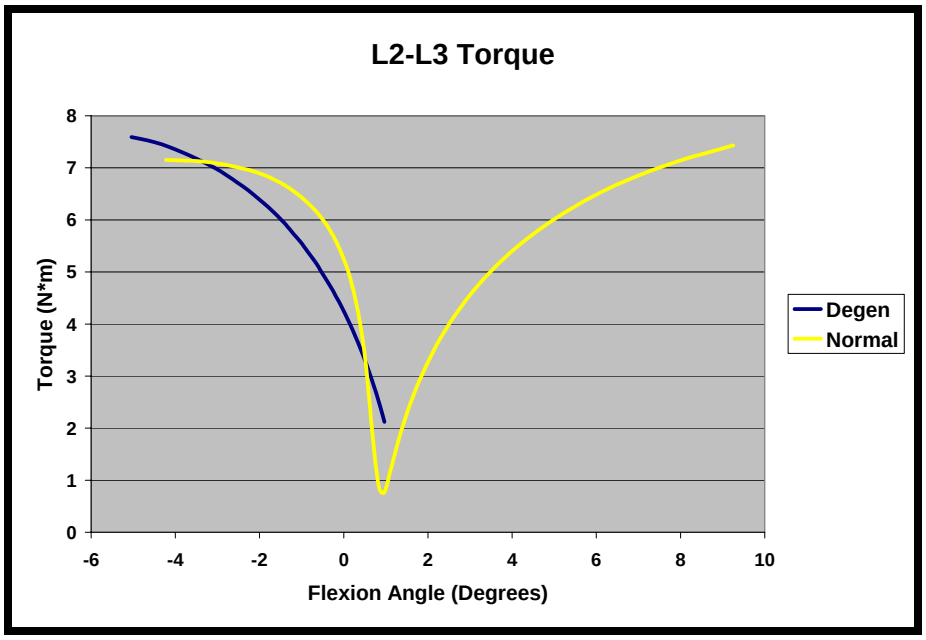

Figure 3-10. Resultant torques between L2 and L3 in the degenerative patient and the normal patient.

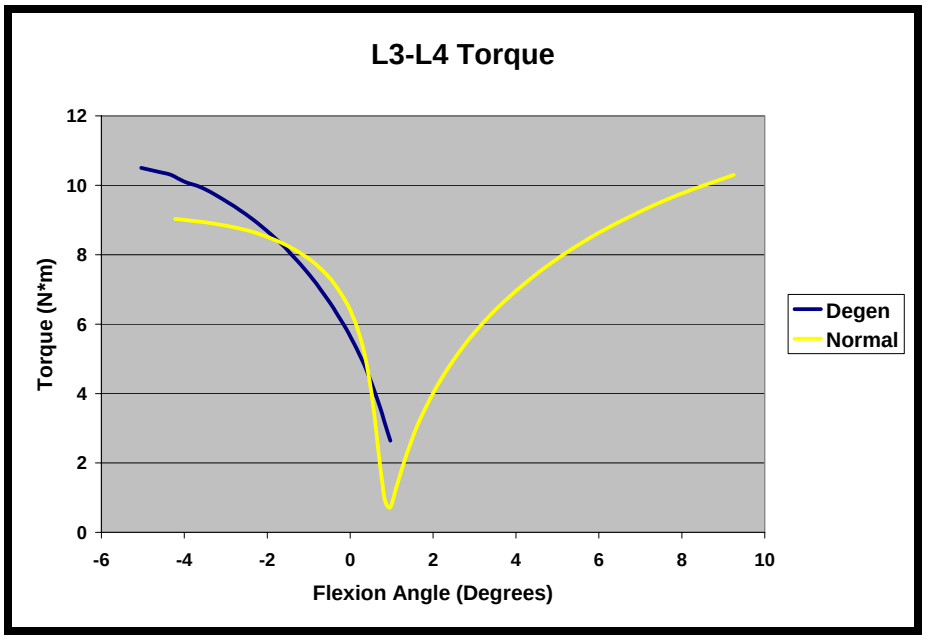

Figure 3-11. Resultant torques between L3 and L4 in the degenerative patient and the normal patient.

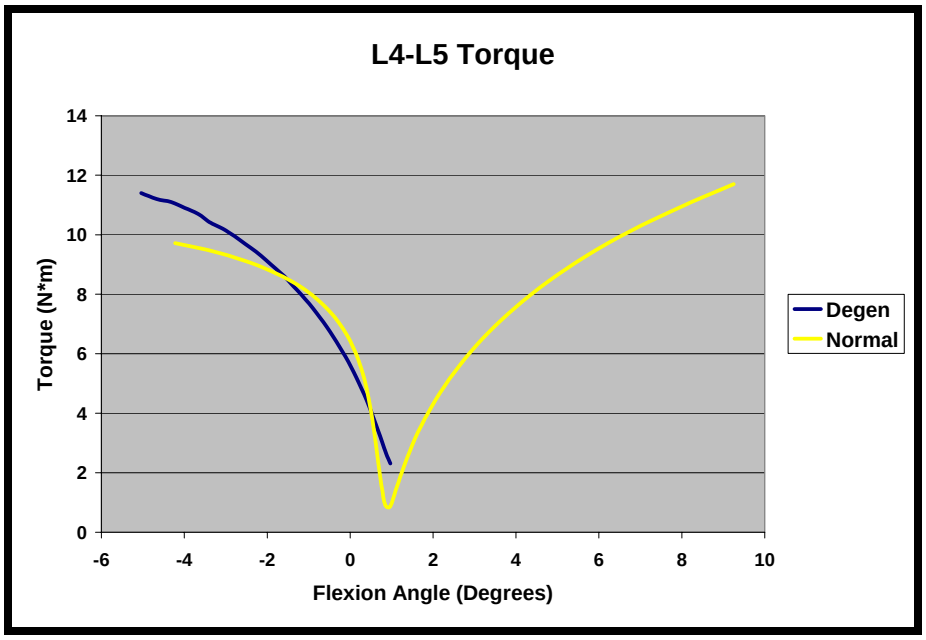

Figure 3-12. Resultant torques between L4 and L5 in the degenerative patient and the normal patient.

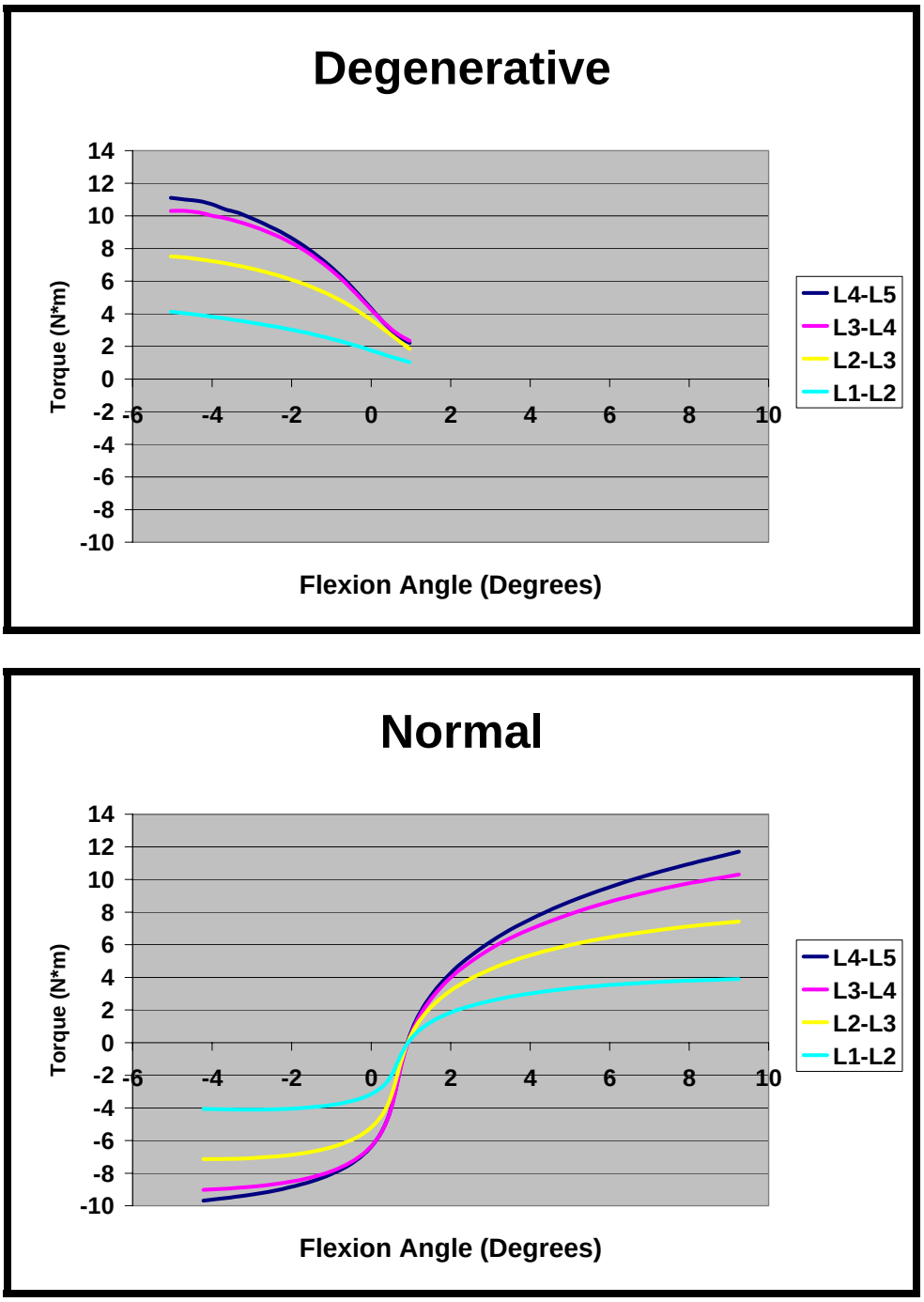

Figure 3-13. Torques around the z axis (3 axis) in the degenerative patient (Top) and the normal patient (Bottom).

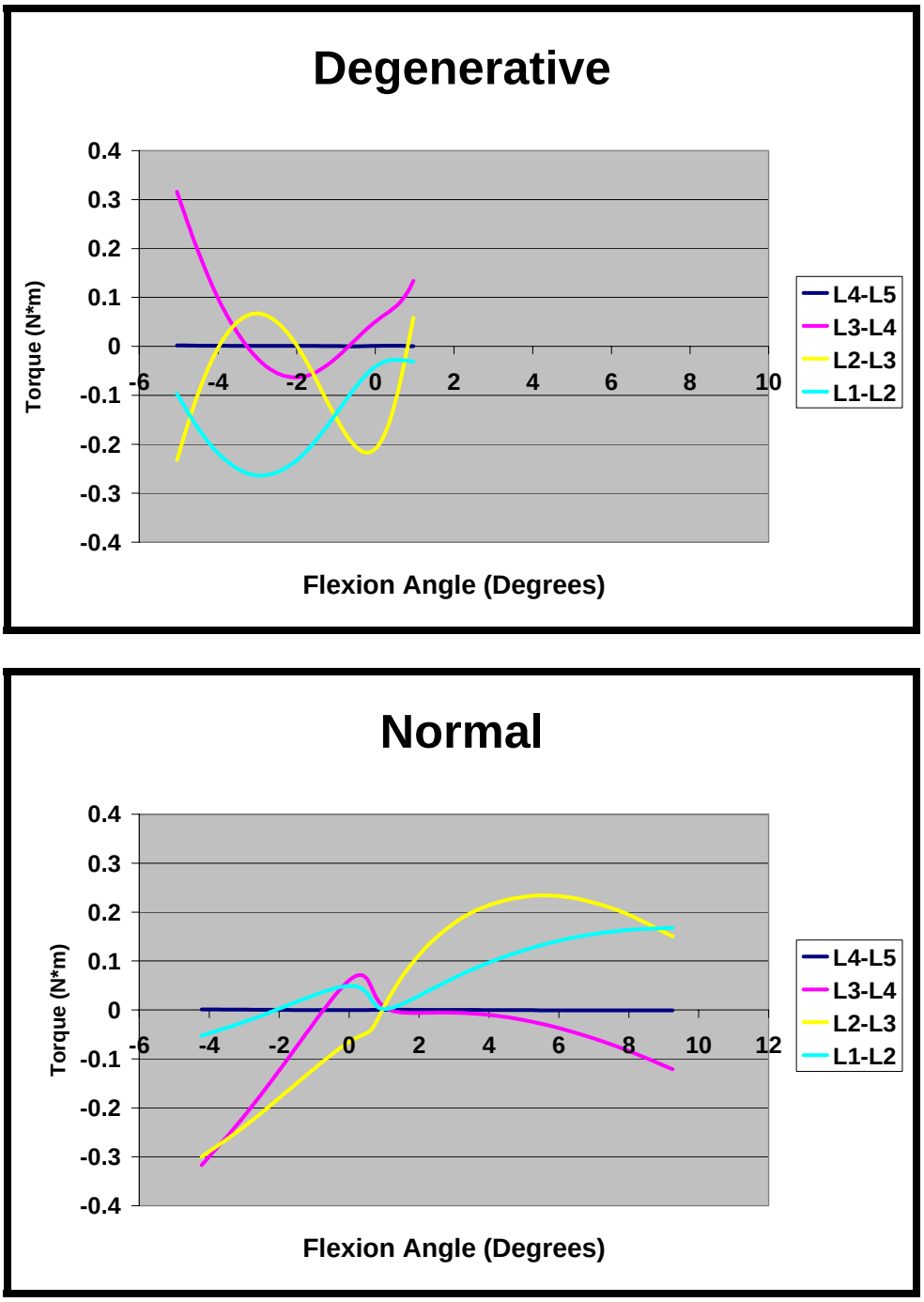

Figure 3-14. Torques around the y axis (2 axis) in the degenerative patient (Top) and the normal patient (Bottom).

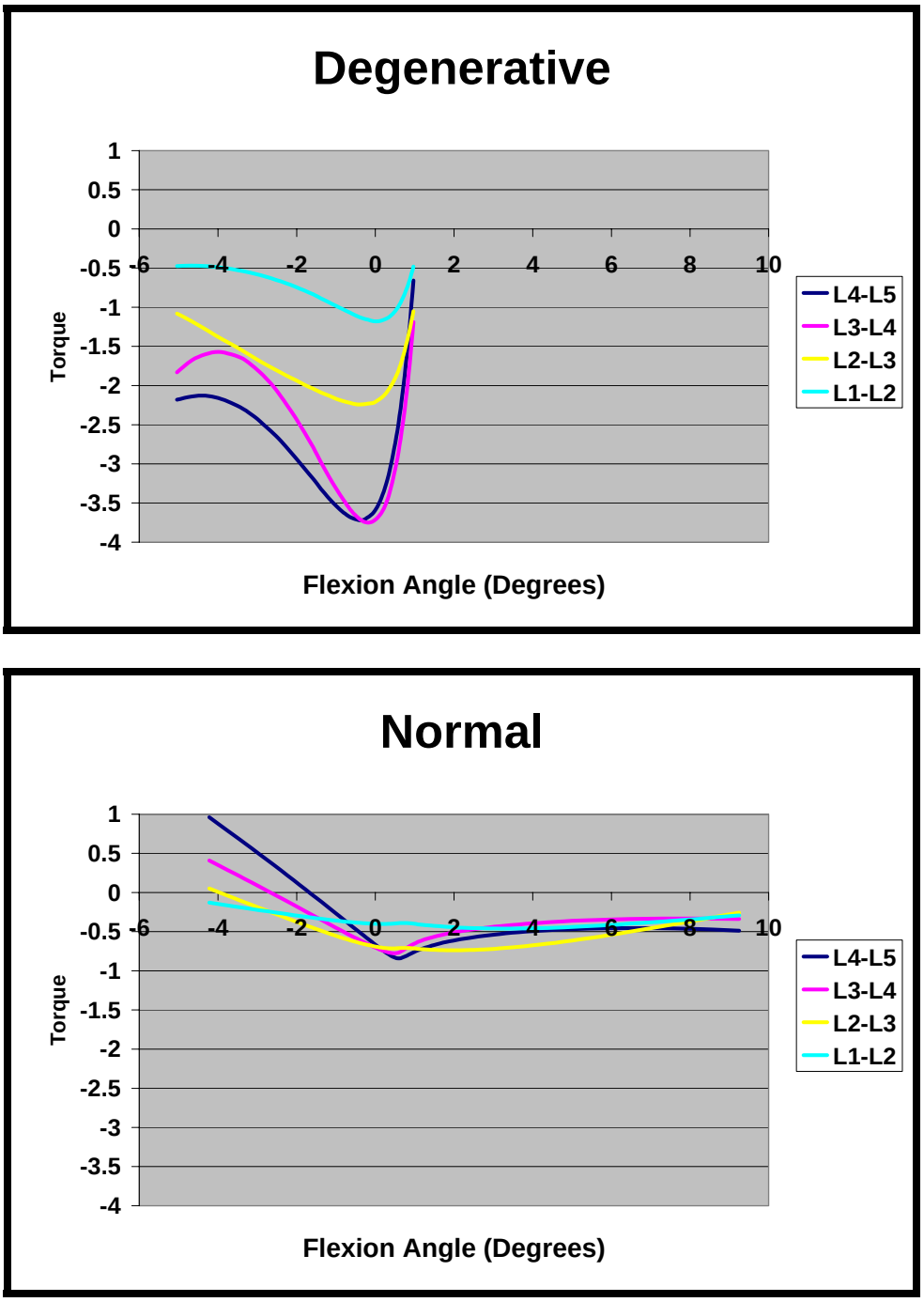

Figure 3-15. Torques around the x axis (1 axis) in the degenerative patient (Top) and the normal patient (Bottom).

Table 2. Resultant torques at 4.22° extension for both patients (maximum extension for the normal patient).

Level	Degenerative	Normal
L1-L2	4.05 N*m	4.07 N*m
L2-L3	7.45 N*m	7.15 N*m
L3-L4	10.3 N*m	9.03 N*m
L4-L5	11.1 N*m	9.72 N*m

The resultant torque at one degree past vertical in the normal patient was 0.422 N*m which was less than the 1.14 N*m at the same point in the degenerative patient (Table 3). The resultant torque increased in the normal patient as the flexion went past one degree and had a maximum 3.91 N*m in full flexion. The degenerative patient did not have a similar increase in flexion because the range of motion was limited.

The torque results for the L2-L3 level can be seen in Figure 3-10. The resultant torque in maximum extension at the L2-L3 level in the degenerative patient was 7.45 N*m and 7.15 N*m in the normal patient (Table 2). The resultant torque in the degenerative patient was 2.12 N*m at the maximum flexion which was nearly one degree past vertical. In the normal patient at the L2-L3 level, the resultant torque at a flexion of one degree past vertical (equivalent to the maximum flexion in the degenerative patient) was 0.769 N*m (Table 3). The resultant torque increased with flexion angle in the normal patient until maximum flexion when the resultant torque reached 7.43 N*m.

Table 3. Resultant torques at one degree past vertical (maximum extension for the degenerative patient).

Level	Degenerative	Normal
L1-L2	1.14 N*m	0.422 N*m
L2-L3	2.12 N*m	0.769 N*m
L3-L4	2.64 N*m	0.725 N*m
L4-L5	2.31 N*m	0.906 N*m

The torque results for the L3-L4 level can be seen in Figure 3-11. At the L3-L4 level, the resultant torque at maximum extension was 10.3 N*m in the degenerative patient and 9.03 N*m in the normal patient (Table 2). The resultant torque at maximum flexion in the degenerative patient was 2.64 N*m. The resultant torque at an equal flexion angle in the normal patient was 0.725 N*m (Table 3). The resultant torque at maximum flexion in the normal patient was 10.3 N*m.

The torque results for the L4-L5 level can be seen in Figure 3-12. At the L4-L5 level, the resultant torque at maximum extension was 11.1 N*m in the degenerative patient and 9.72 N*m in the normal patient (Table 2). The resultant torque at maximum flexion in the degenerative patient was 2.31 N*m. The resultant torque in the normal subject at a flexion angle equal to the max flexion in the degenerative subject was 0.906 N*m. At maximum flexion in the normal patient, the resultant torque was 11.7 N*m (Table 3).

The torques around the z axis (3 axis) are the highest torques and they dominate the resultant torque results (Figure 3-13). The torques around the y axis (2 axis) were very small (Figure 3-14). The torques in the normal and degenerative patient were all under 0.3 Newton meters. The torques around the x axis (1 axis) were significantly different. The torques were much higher around this axis in the degenerative patient as compared to the normal (Figure 3-15). The maximum torques around the x axis at the L3-L4 and L4-L5 level were 3.75 N*m in the degenerative patient and 1 N*m or less in the normal patient. The maximum torque around the x axis at the L2-L3 level was 2.75 N*m in the degenerative patient and 0.7 N*m in the normal patient. The maximum torque around the x axis at the L1-L2 level was 1.25 N*m in the degenerative patient and 0.5 N*m in the normal patient.

The lowest torques are at 1.0 degree of flexion. The torques are lowest at this point because the moment arm is the smallest. The reason that this occurs at 1.0 degrees of flexion instead of 0 degrees of flexion is the flexion angle is the angle between L4 and L5 and when that angle is zero, the other levels of the spine are not yet vertical. The higher levels are nearer to vertical when the angle between L4 and L5 is 1.0 degrees past vertical.

3.3 Sensitivity Analysis

The results from the sensitivity analysis determine that the most sensitive parameter was the input kinematic data. Altering the input kinematic data could lead to significant

changes in the output kinetic data predicted by the model. On contrary, changing the variable contact points and the inertial values altered the kinetic data only minimally.

4 DISCUSSION

4.1 Kinematics

This thesis describes a computational model to predict *in vivo* contact forces and body torques in the lumbar vertebrae, L1-L5. An inverse dynamics mathematical model was created to solve for the unknown forces in the system using the reduction method. The most sensitive input to the model is the kinematic data from the fluoroscopy and the 2D to 3D registration process. The definitions of the variable contact points, masses and inertia of the vertebrae do not affect the force results nearly as much. It is very important to have the 3D kinematics accurately defined so the input equations for the rotations and translations of the vertebrae. The accuracy of the 2D to 3D registration is very important to the results of the mathematical model. For this study, one normal and one degenerative patient were compared.

The kinematic results show that the sagittal range of motion (around the z axis) in the degenerative patient was much smaller than in the normal patient. The degenerative patient may not have had an equivalent range of motion due to the pain involved in the activity. The patient may have stopped flexing at the onset of pain, or the patient may have compensated by flexing at the hip instead of using the lumbar spine to flex. The range of motion in the other two directions, around the x and y axes was greater in the degenerative patient than in the normal patient. These results may show instability in the lumbar spine of the degenerative patient, because it has been shown previously that degenerative changes in the lumbar spine can lead to increased range of motion in axial rotation and lateral bending (Panjabi, 2003; Abumi, et al., 1990). Spinal instability can

be caused by an abnormality in any of three components: the spinal column, the muscles surrounding the spinal column, or the neural control unit (Panjabi, 2003). Spondylolisthesis has been associated with instability in several studies (Frymoyer and Selby, 1985; Nachemson, 1985).

4.2 Kinetics

The results for the forces in the normal and degenerative patients were very similar. The maximum vertical forces were nearly identical in both patients. The forces are relative to body weight and the forces ranged from 0.415*BW to 0.365*BW. This is reasonable since the external input force applied at L1 was 0.4*BW. This input force represented the weight of the upper body above L1. The vertical force at the L4 – L5 level was 0.42 *BW in both the degenerative and the normal patient. The vertical forces are constant at L5 since L5 is fixed in the model. The maximum vertical forces decreased slightly at each higher level because there is less body weight at each higher level. The vertical forces in the normal patient decreased through flexion which did not occur in the degenerative patient since the range of motion was much smaller and the flexion angle did not go more than 1.0 degree past vertical.

The forces in the transverse directions were also similar in both patients. The forces in the z direction (3 direction) were small in both patients. The forces in the x direction (1 direction) were largest at maximum extension in both patients and at maximum flexion in the normal patient and smallest through the neutral region. This is logical since the vertical force dominates around the neutral region when the spine is more vertical.

The interactive contact forces found in this study are slightly lower than the forces found by Nachemson et al. Nachemson reported forces of 1.1*BW in a standing subject in flexion. Ledet et al. found higher forces in their animal model of up to greater than 2.5*BW. Rohlmann et al. reported forces that were similar to the forces found in the model in this thesis. The forces measured were between 0 and 0.6*BW for all of the patients.

The differences could be due to the fact that the only external force in the model was the applied force at L1 that represented the weight of the upper body. Adding an external force at L5 to represent the ground reaction force would also increase the vertical forces found in the model described in this thesis. The differences in the reported muscle forces could also be due to the methods of measuring the forces within the spine. Nachemson et al. and Ledet et al. measured forces with an implant in the intervertebral disc space. In the studies by Rohlmann et al. the forces were measured within a spinal fixator which is more posterior than the intervertebral disc. None of these previous studies modeled a variable contact position between the vertebrae so the forces were being measure at one point that was not the contact point throughout the entire range of motion. The muscle forces are not solved for directly in this model. The muscle forces are accounted for in the body torques.

The torques at the L1-L2 level are very similar in the normal and degenerative patient. The differences are more evident at each lower level. The largest differences are in L4-L5. This is logical since the degenerative patient had spondylolisthesis of L5 onto S1 so the degeneration is at that level. The anatomy and motions of the L1-L2 level would not be affected as greatly as the lower levels by the degeneration at L5, so the

kinetic differences in the normal and degenerative patient would not be as large at L1-L2. The largest differences show up at the L4 – L5 level where there was a 1.4 N*m difference in the torque values in the normal and degenerative patients at maximum extension.

The difference in the range of motion around the z axis in the normal and degenerative patient gives rise to the differences in shape of the graphs. If degenerative patient extended to the same range of motion as the normal patient, the torques would most likely be higher in flexion just as they were higher at maximum extension and at one degree past vertical. The torques around the z axis (3 axis) experienced by the degenerative patient were higher at maximum extension than the torques experienced by the normal patient. The maximum flexion for the degenerative patient was 1.0 degree past vertical. The torques at one degree of flexion were higher in the degenerative patient than in the normal patient.

The torques around the x axis (1axis) were also significantly higher in the degenerative patient as compared to the normal patient. This is a result of the instability in the lumbar spine of the degenerative patient. This instability can be seen in the kinematic results (Figures 3-4 and 3-5). The greater range of motion around this axis in the degenerative patient leads to the higher calculated torques.

The torques predicted using our model were slightly higher than torques in other studies throughout the range of motion. Rohlmann et al. reported torques up to 8 Newton meters in extension. The torques predicted for the lumbar spine in this thesis were slightly higher and were up to 11.1 Newton meters at the L4-L5 level. Unfortunately, Rohlmann did not report torques at the L4-L5 level, which didn't allow us to conduct a

direct comparison with the results from his study. Two patients in our study had L3 bridged and one patient had L4 bridged by the internal spinal fixation device. The torques would most likely be higher if measured at the lower level. The published data reports torques found in telemeterized implants or in cadavers. These numbers may not be an accurate representation of the true *in vivo* torque values because the implanted cage, interbody device or spinal fixator can alter the biomechanics. The patients in this study were not implanted with any fixation device, so the torques calculated are more accurate for *in vivo* conditions.

The muscle forces in this model are not solved for directly, but they are accounted for in the torques. The torques in this study may be higher than the forces found in other studies because they account for the muscle forces. The torques found in other studies are directly measured and do not account for the muscle forces that cannot be measured since the muscles are cut or there is not a direct method of measurement.

4.3 Future Work

This thesis was an initial step in the model to determine and compare forces and torques in normal and degenerative lumbar spines. The results that were shown were only for one normal and one degenerative patient, and should not be generalized for all subjects having a normal or degenerative lumbar spine. The created model can be applied to any patient that has undergone fluoroscopic examination and CT scanning. The registration software is being updated to output the kinematics automatically which will allow the model to be more easily applied to a large number of patients without the tedious process of the user manually determining the kinematic equations. More images

could easily be captured an analyzed throughout the motion which may improve the kinematic input into the mathematical model.

In the future, the model will be extended and muscle and ligament forces may be added. This could be done by locating the attachment sites of the muscles and ligaments and then by modeling them as springs. The system could be kept determinate by adding more bodies to the system. The posterior elements of the vertebrae could be modeled as separate bodies and micro motions could be added between the different portions of the vertebrae and then constrained later in the model. The discs themselves were not included in this initial model, but may be added in the future. This could be done using finite element methods to model the deformation within the discs under loading.

The contact between the vertebrae may also be changed to better account for the load sharing between the vertebral body and the two facet joints. Each vertebral level has three areas of interaction; the two facet joints and the intervertebral disc (White and Panjabi, 1990). The facets and posterior portion of the vertebral body carry most of the load in extension, but the majority of the load is transferred to the vertebral body through flexion. It has been reported that increasing degeneration in the lumbar spine leads to increasing load across the posterior elements of the vertebrae in extension (Niosi and Oxland, 2004). This load sharing could be accounted for in the future by adding contact points that would represent the facet joints. A switch in the model could allow the model to represent the forces across the facets in extension and then shift the load to the vertebral body or disc through flexion.

A variable input force predicted at the hip joint by modeling the whole lower extremity may may lead to more accurate lumbar spine forces. This would help in

overcoming the limitation of a constant input force that is applied in the current model. The lack of an input torque as a result of the weight of the upper body is another limitation. This torque could be included by finding the center of mass of the upper body and applying the input force at this location. Currently, the input force is applied directly to the superior surface of the L1 vertebra which is not the exact location of the center of mass of the upper body.

REFERENCES

References

1. Abumi, K, Panjabi, M.M., Kramer, K.M. *Biomechanical evaluation of lumbar spine stability after graded facetectomies*. Spine 15 (1990). 1142-1147.
2. Andriacchi, T., Alexander, E., Toney, M., Dyrby, C., Sum, J. *A point cluster method for in vivo motion analysis: applied to a study of knee kinematics*. Journal of Biomedical Engineering. 120(6). pp 743-749. 1998.
3. Banks, S.A. and Hodge, W.A. *Accurate measurement of three-dimensional knee replacement kinematics using single-plane fluoroscopy*. IEEE Transactions in Biomedical Engineering, 1996. 43(6): p.638-49.
4. Bergmann, G., Graichen, F., Rohlmann, A., 1993. *Hip joint loading during walking and running, measured in two patients*. Journal of Biomechanics 26, 969–990.
5. Bergmann, G., Graichen, F., Rohlmann, A., Dipl-Ing, H.L., 1997. *Hip joint forces during load carrying*. Clinical Orthopaedic Related Research 335, 190–201.
6. Cappazzo, A. *Three-dimensional analysis of human walking: Experimental methods and associated artifacts*. Human Movement Science, Vol 10, (1991) 589-602.
7. Cheze, L. *Comparison of different calculations of three-dimensional joint kinematics from video-based system data*. Journal of Biomechanics, Vol 33, 1695-1699. 2000.
8. Crosbie, J. et al. *Gait and Posture*, 5, 6-12, 1997.
9. Davy, D.T., Kotzar, G.M., Brown, R.H., Heiple, K.G., Goldberg, V.M., Heiple Jr., K.G., Berilla, J., Burstein, A.H., 1988. *Telemetric force measurements across*

the hip after total arthroplasty. Journal of Bone and Joint Surgery 70-A (1), 45–50.

10. Dennis, D.A., Komistek, R.D., Colwell, C.E., Ranawat, C.S., Scott, R.D., Thornhill, T.S., Lapp, M.A. *In vivo anteroposterior femorotibial translation of total knee arthroplasty: a multicenter analysis*. Clinical Orthopedics, 356. 47-57. 1998.
11. Dooris, A., Goel, V., Grosland, N., Gilbertson, L., Wilder, D. *Load-sharing between anterior and posterior elements in a lumbar spine motion segment implanted with an artificial disc*. Spine (26) 6. pp E122-E129.
12. Etebar, S., Cahill, D.W., *Risk factors for adjacent-segment failure following lumbar fixation with rigid instrumentation for degenerative instability*. Journal of Neurosurgery (Spine 2) 90: 163-169, 1999.
13. Frymoyer, J.W., Selby, D.K. *Segmental instability: rationale for treatment*. Spine 10 (1985). 280-286.
14. Goto, K., Tajima, N., Chosa, E., Totoribe, K., Kubo, S., Kuroki, H., Arai, T. *Effects of lumbar spinal fusion on the other lumbar intervertebral levels*. J. Orthop Sci (2003). 8: 577-584.
15. Gunnarsson, G., Axelsson, P., Johnnson R., Strömqvist, B. *A Method to Evaluate the in vivo Behaviour of Lumbar Spine Implants*. European Spine Journal (2000). 9: 230-234.
16. Hoff, W.A., Komistek, R.D., Dennis, D.A., Gabriel, S.M., Walker, S.A. *Three-Dimensional Determination of Femoral-Tibial Contact Positions under In Vivo Conditions using Fluoroscopy*. Clinical Biomechanics 13, 455-472.

17. Huston, Ronald L., *Multibody Dynamics*. Butterworth-Heinemann. 1990.

18. Johnsson, R., Axelsson, P., Gunnarsson, G., Strömqvist, B. *Stability of Lumbar Fusion with Transpedicular Fixation Determined by Roentgen Stereophotogrammetric Analysis*. Spine. 24 (7). Pp 687-690. 1999.

19. Kane, T.R., Levinson, D.A. (1983). *Formulation of equations of motion for complex spacecraft*. Journal of Guidance and Control 3 (2), 99-112.

20. Kane, T.R., Levinson, D.A. (1985). **Dynamics: Theory and Applications**. New York: McGraw-Hill Publishing Company.

21. Kane, T.R., Levinson, D.A., **Dynamics Online: Theory and Implementation with Autolev™**. ©2000.

22. Kaufman, K.R., Kovacevic, N., Irby, S.E., Colwell, C.W. *Instrumented implant for measuring tibiofemoral forces*. Journal of Biomechanics 29, 667–671. 1996.

23. Kelsey, J.L., White, A.A. Epidemiology *and Impact of Low-Back Pain*. Spine, 1980. 5(2). P. 133-142.

24. Komistek, R.D., Kane, T.R., Mahfouz, M.R., Ochoa, J.A., Dennis, D.A. *Knee Mechanics: a review of past and present techniques to determine in vivo loads*. Journal of Biomechanics. 38, 215-228. 2005.

25. LaFortune, M.A., Cavanagh, P.R., Sommer, H.J., Kalenak, A. *Three-Dimensional Kinematics of the Human Leg During Walking.* Journal of Biomechanics 25, 347-357. 1992.

26. Ledet, Eric H. Tymeson Michael P. DiRisio, Darryl J. Cohen, Benjamin. Uhl, Richard L. *Direct real-time measurement of in vivo forces in the lumbar spine*. The Spine Journal 5 (2005) 85-94.

27. Luo, X., Pietroban, R., Sun, S., Liu, G., Hey, L. *Estimates and Patterns of Direct Health Care Expenditures Among Individuals With Back Pain in the United States*. Spine. 2004. 29(1). P. 79-86.
28. Mahfouz, M., W. Hoff, R. Komistek, and D. Dennis, *A Robust Method for Registration of Three-Dimensional Knee Implant Models to Two-Dimensional Fluoroscopy Images*. IEEE Trans. Medical Imaging, Vol. 22, No. 12, pp. 1561-74, 2003.
29. Murphy, M., 1990. Geometry and the kinematics of the normal human knee. Ph.D. Thesis, Department of Mechanical Engineering, Massachusetts Institute of Technology.
30. Nachemson, A. *The load on lumbar disks in different positions of the body*. Clinical Orthopedics and Related Research. 1966. 45. pp.107-122.
31. Nachemson, A. *Lumbar spine instability: a critical update and symposium summary*. Spine 10 (1985). 290-291.
32. National Center for Health Statistics
33. National Institute for Neurological Disorders and Stroke. http://www.ninds.nih.gov/disorders/backpain/
34. Niosi, C., Oxland, T. *Degenerative mechanics of the lumbar spine*. The Spine Journal 4 (2004). 202S-208S.
35. North American Spine Society, 2000. http://www.spine.org/articles/spondylolisthesis.cfm

36. Pape, D.,Adam, F., Fritsch, E., Müller, K., Kohn, D. *Primary Lumbosacral Stability after Open Posterior and Endoscopic Anterior Fusion With Interbody Implants*. Spine. 25(19). pp 2514 – 2518, 2000.
37. Panjabi, M.M. *Clinical spinal instability and low back pain*. Journal of Electromyography and Kinesiology 13(2003). 371-379.
38. Pratt, W.K., **Digital Image Processing. 2nd ed**. 1991, New York: Wiley & Sons.
39. Ramsey, D.K., Wretenberg, P.F., Benoit, D.L., Lamontagne, M., Németh, G. *Methodological concerns using intra-cortical pins to measure tibiofemoral kinematics*. Knee Surgery, Sports Traumatology, Arthroscopy 11(5). 344-349. 2003.
40. Roberts M.P.: Complications of lumbar disc surgery. In: Hardy RW Jr, ed. Lumbar Disc Disease. 2nd Ed. New York: Raven, 161-169, 1993.
41. Rogers, B., Wiese, S., Blackenbaker, D., Meyerand, E., Haughton, V. *Accuracy of an Automated Method to Measure Rotations of Vertebrae from Computerized Topography Data.* Spine. Volume 30(6). 694-696. 2005.
42. Rohlmann, A., Bergmann, G., Graichen, F., Weber, U. *Comparison of loads on internal spinal fixation devices measured in vitro and in vivo*. Med. Eng. Phys. Vol. 19, No. 6, pp. 539-546, 1997.
43. Rowe, P.J., White, M. *Gait and Posture*, 4, 242-251, 1996.
44. Soutas-Little, R., Beavis, G., Verstraete, M., Markus, T. Analysis of foot motion during running using a joint coordinate system. Medicine and Science in Sports and Exercise. 19(3). pp 285-293. 1987.

45. Taylor, V.M., Deyo, R.A., Cherkin, D.C., Kreuter W. *Low back pain hospitalization: Recent United States trends and regional variations*. Spine. 1994;19(11):1207-1213.

46. Taylor, S.J.G., Walker, P.S., Perry, J.S., Cannon, S.R.,Woledge, R. *The forces in the distal femur and the knee during walking and other activities measured by telemetry*. Journal of Arthroplasty 13, 428–437. 1998.

47. Taylor, S.J.G., Walker, P.S. *Forces and moments telemeterized from two distal femoral replacements during various activities*. Journal of Biomechanics 839–848. 2001.

48. Throckmorton, T.W., Hilibrand, A.S., Mencio, G.A., Hodgre, A., Spengler, D.M., *The impact of adjacent level disc degeneration on health status outcomes following lumbar fusion*. Spine 28(22). 2546-2550. 2003.

49. Weinstein P.R.: Lumbar stenosis. In: Hardy RW Jr., ed. Lumbar Disc Disease. 2nd Ed. New York: Raven, 241-255, 1993.

50. White A.A. III, Panjabi M.M. **Clinical Biomechanics of the Spine**. 2nd ed. Philadelphia: JB Lippincott, 1990.

51. Whittle, M.W., Levine, D.F. *Gait and Posture*, 5, 101-107, 1997.

52. Winter, David A., **Biomechanics and Motor Control of Human Movement** 2nd Ed. New York: Wiley-Interscience, 56-57, 1990.

53. World Health Organization

APPENDICES

Appendices

Appendix A-Curve-fitting of Rotations and Translations

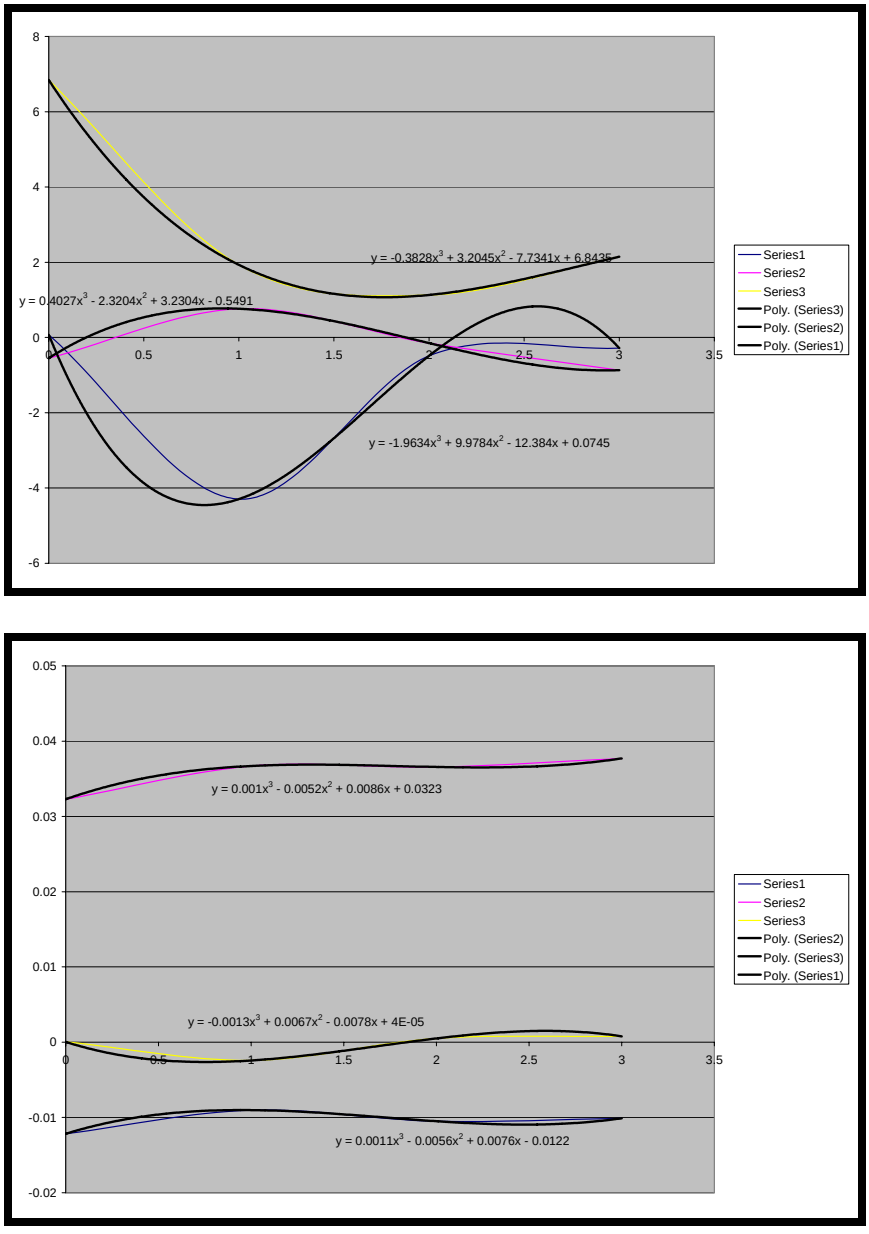

Figure A-1. Curve-fitting of the rotations (Top) and translations (Bottom) for L1-L2 in the degenerative patient.

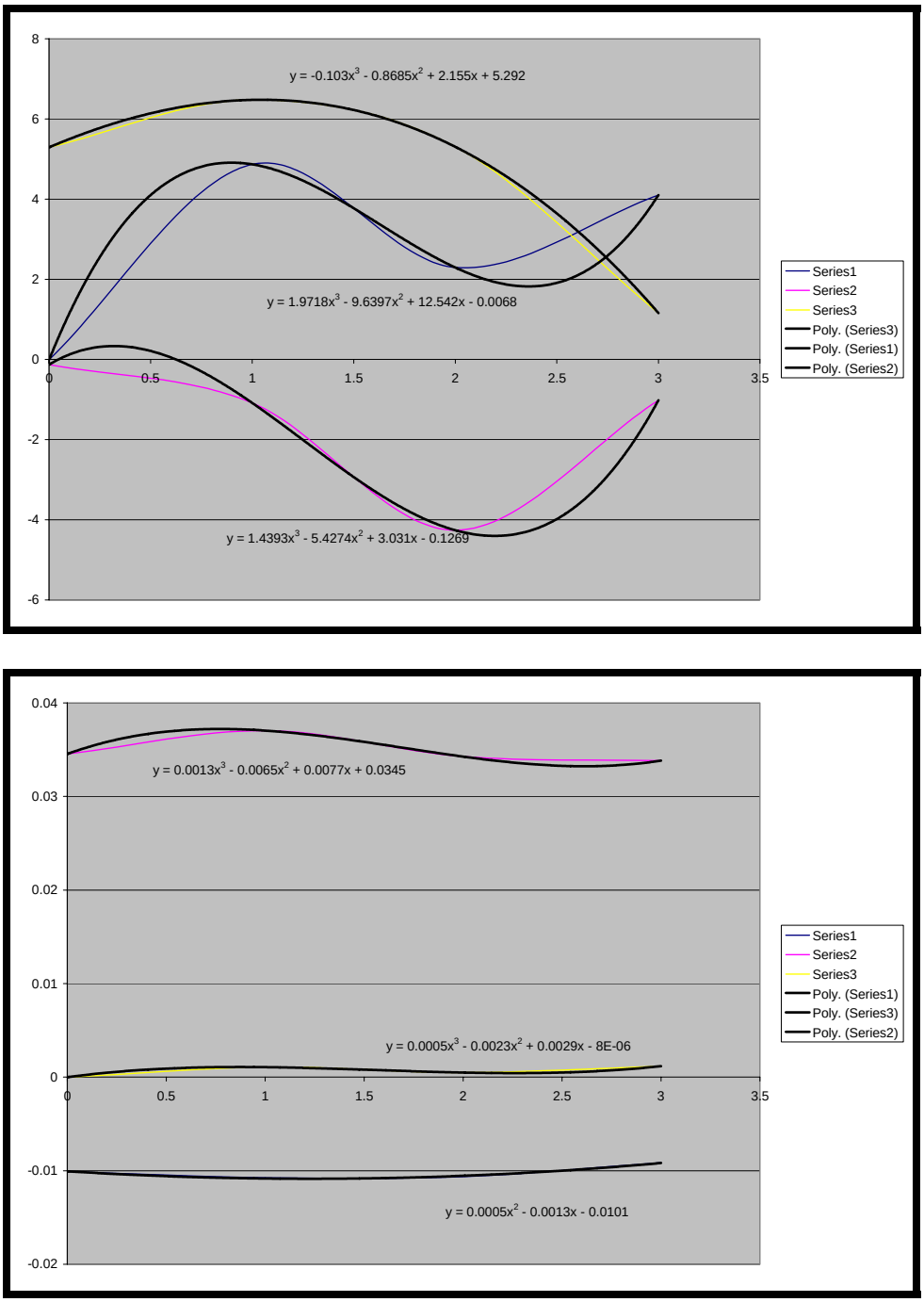

Figure A-2. Curve-fitting of the rotations (Top) and translations (Bottom) for L2-L3 in the degenerative patient.

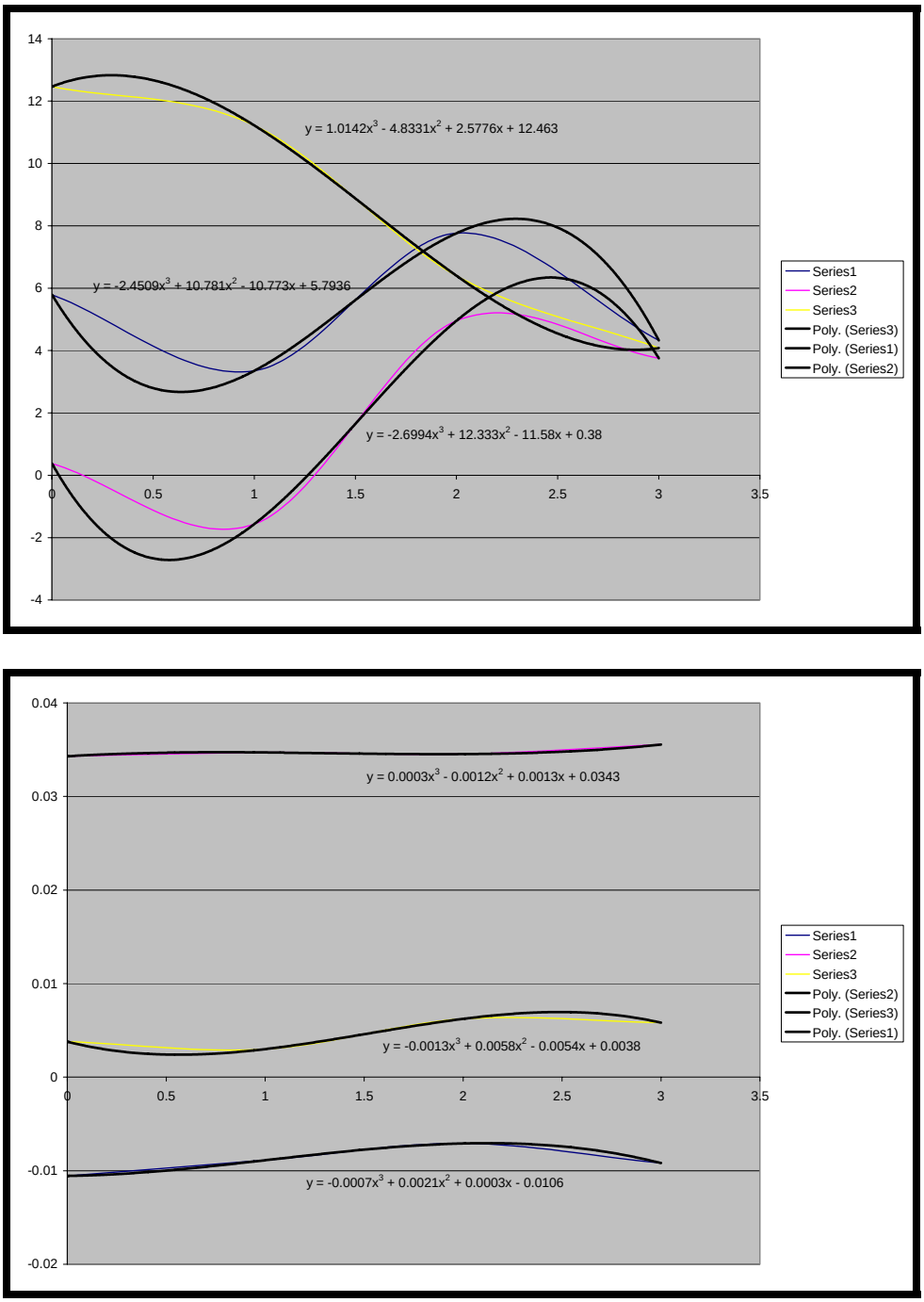

Figure A-3. Curve-fitting of the rotations (Top) and translations (Bottom) for L3-L4 in the degenerative patient.

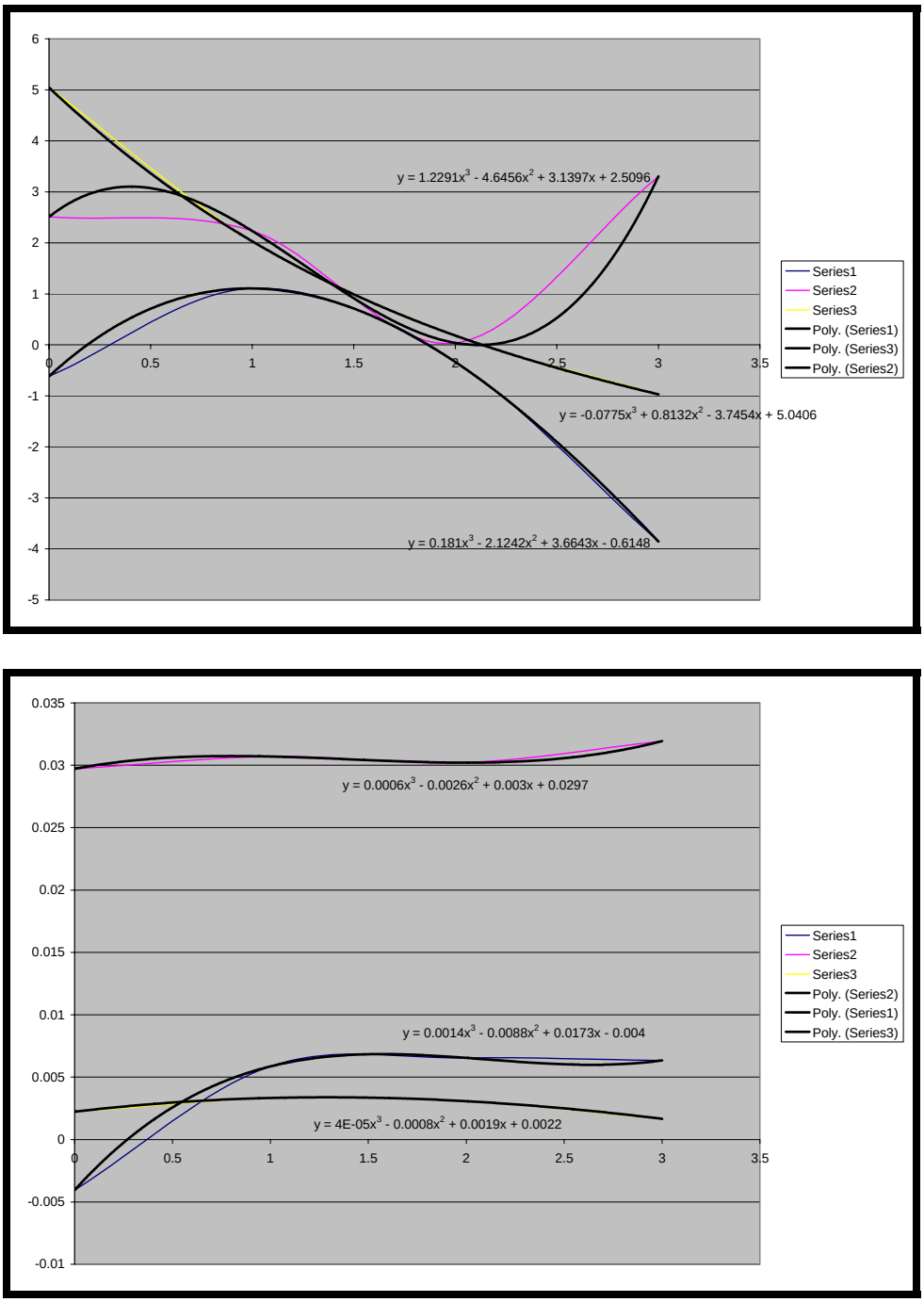

Figure A-4. Curve-fitting of the rotations (Top) and translations (Bottom) for L4-L5 in the degenerative patient.

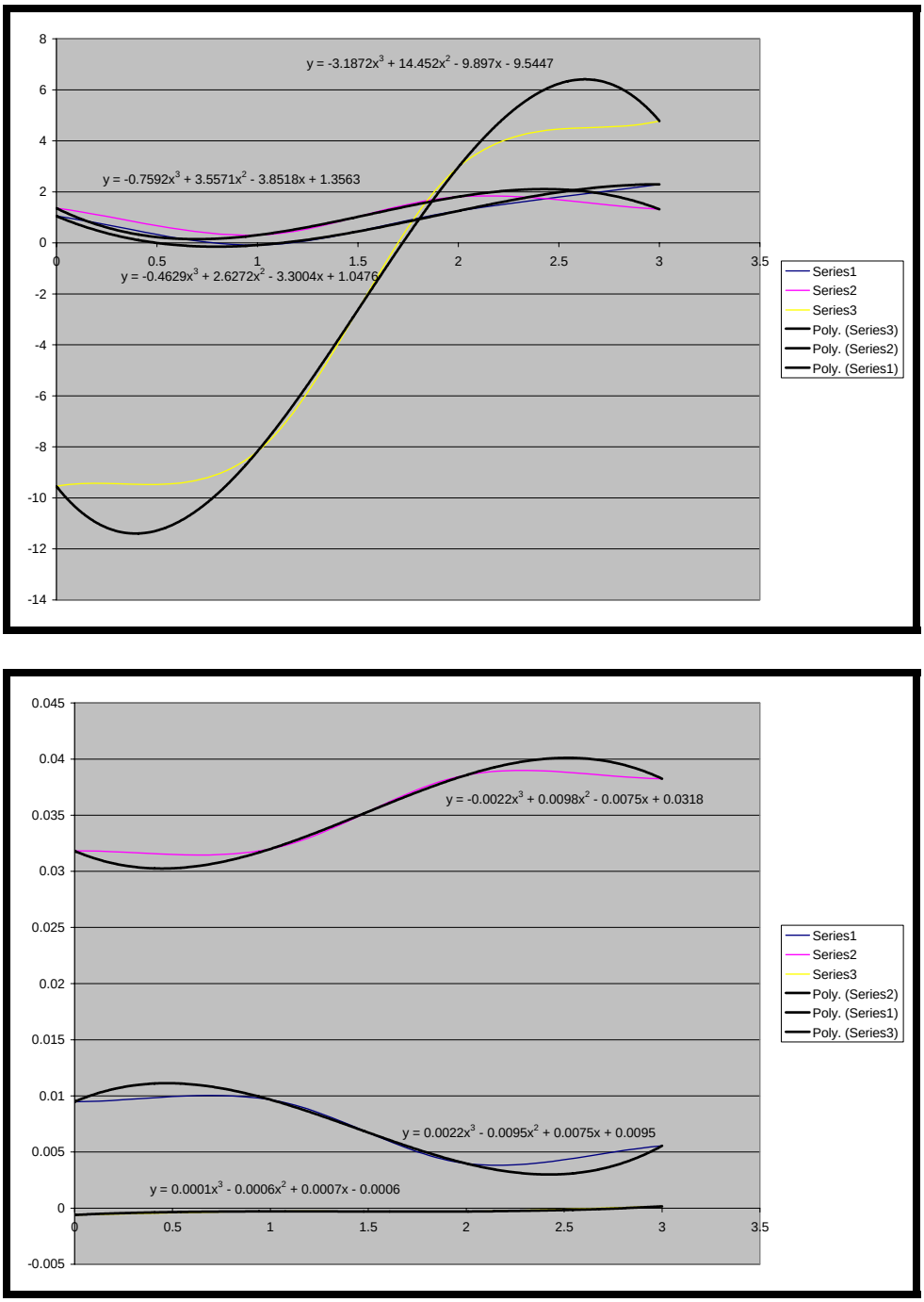

Figure A-5. Curve-fitting of the rotations (Top) and translations (Bottom) for L1-L2 in the normal patient.

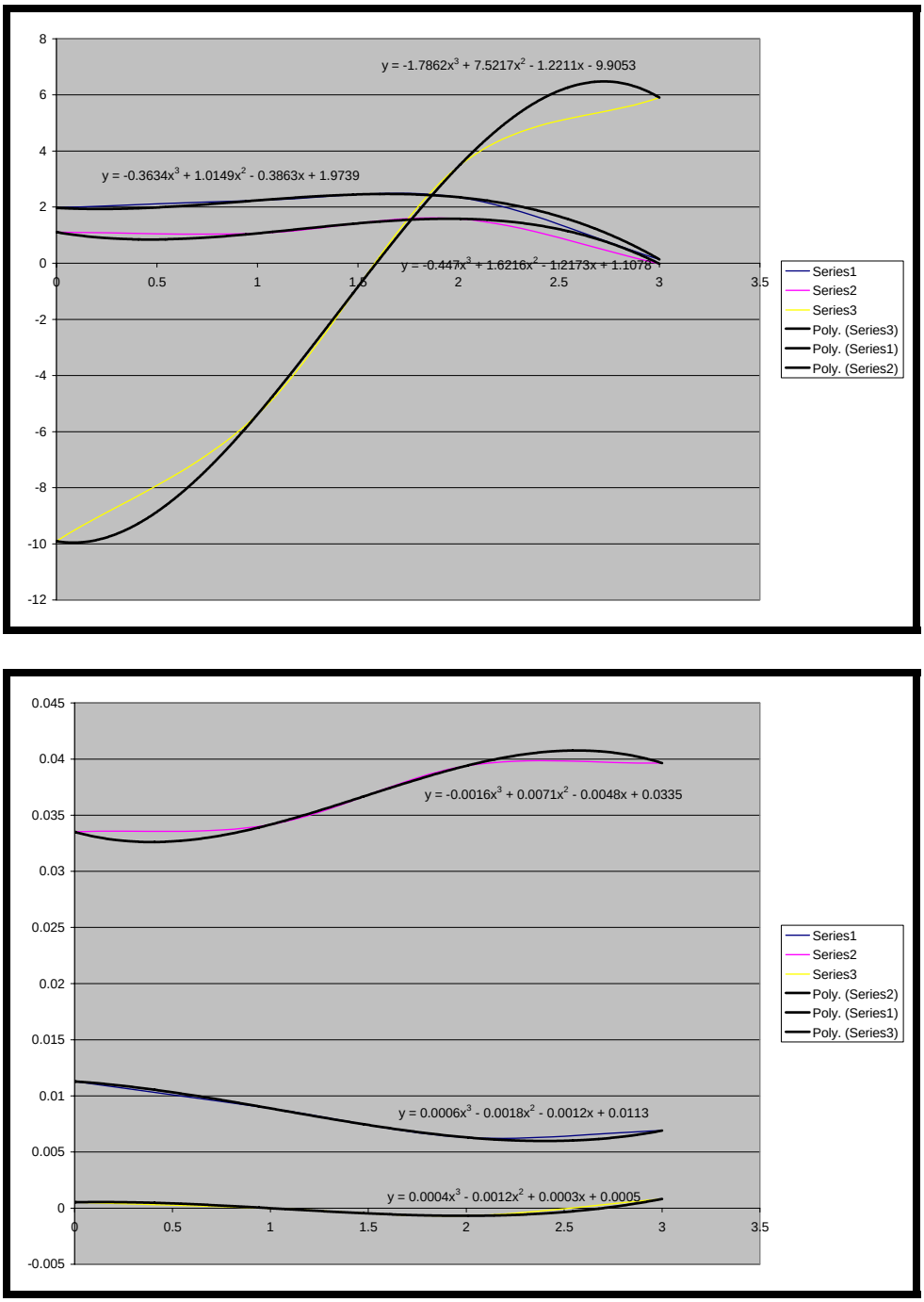

Figure A-6. Curve-fitting of the rotations (Top) and translations (Bottom) for L2-L3 in the normal patient.

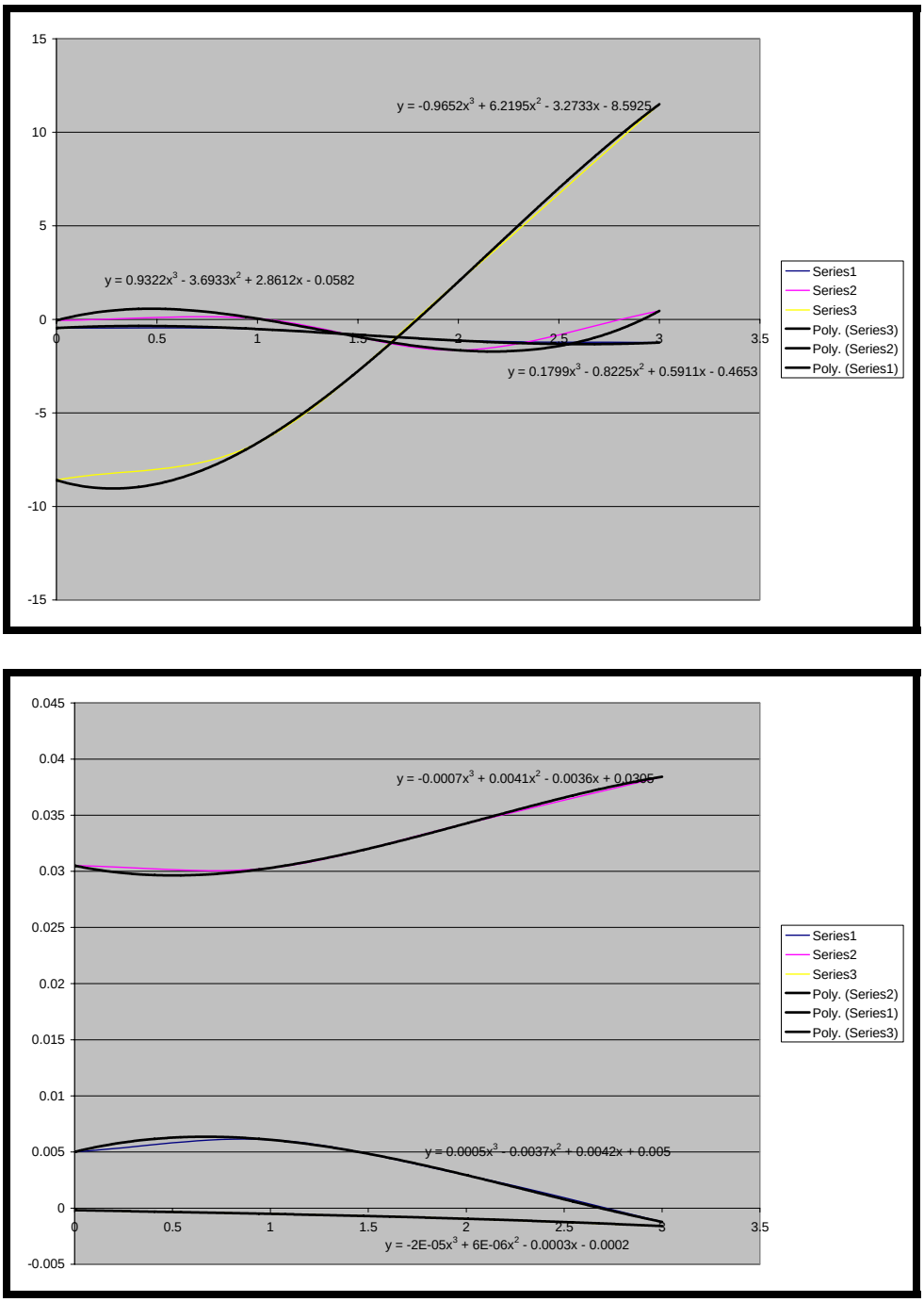

Figure A-7. Curve-fitting of the rotations (Top) and translations (Bottom) for L3-L4 in the normal patient.

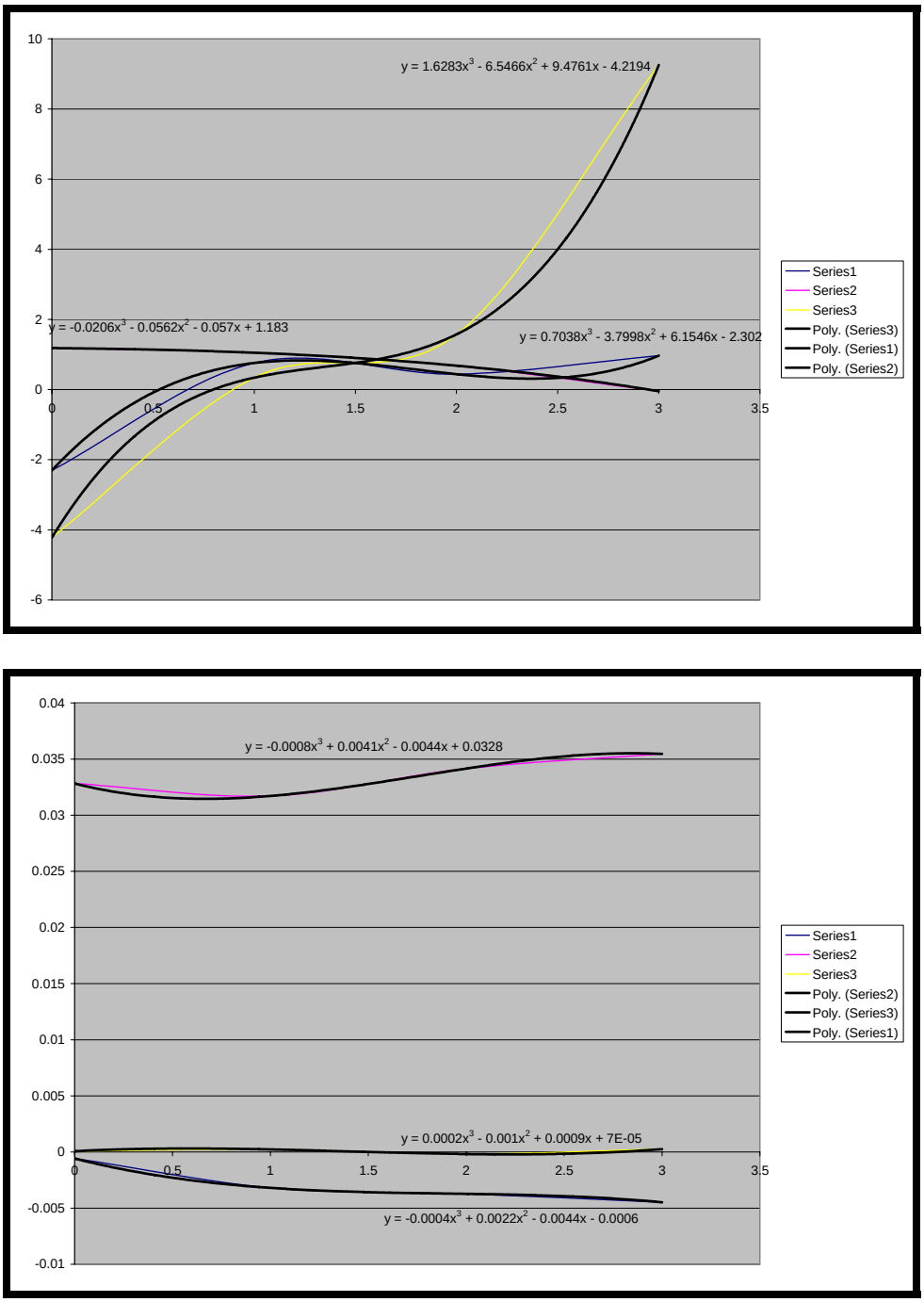

Figure A-8. Curve-fitting of the rotations (Top) and translations (Bottom) for L4-L5 in the normal patient.

Appendix B-Kinetic Results vs. Normalized Time

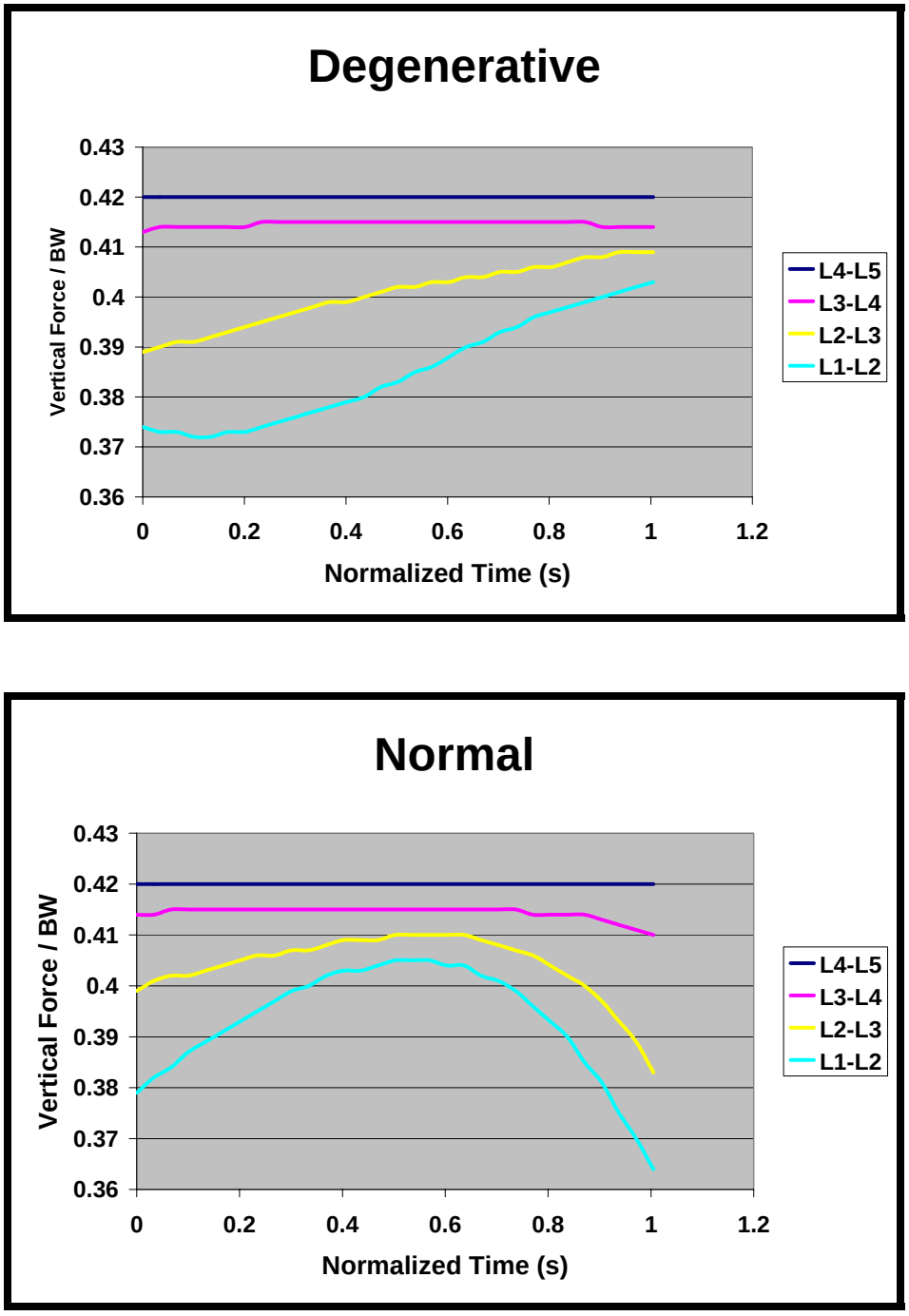

Figure B-1. Vertical forces at every level for the degenerative patient (Top) and the normal patient (Bottom).

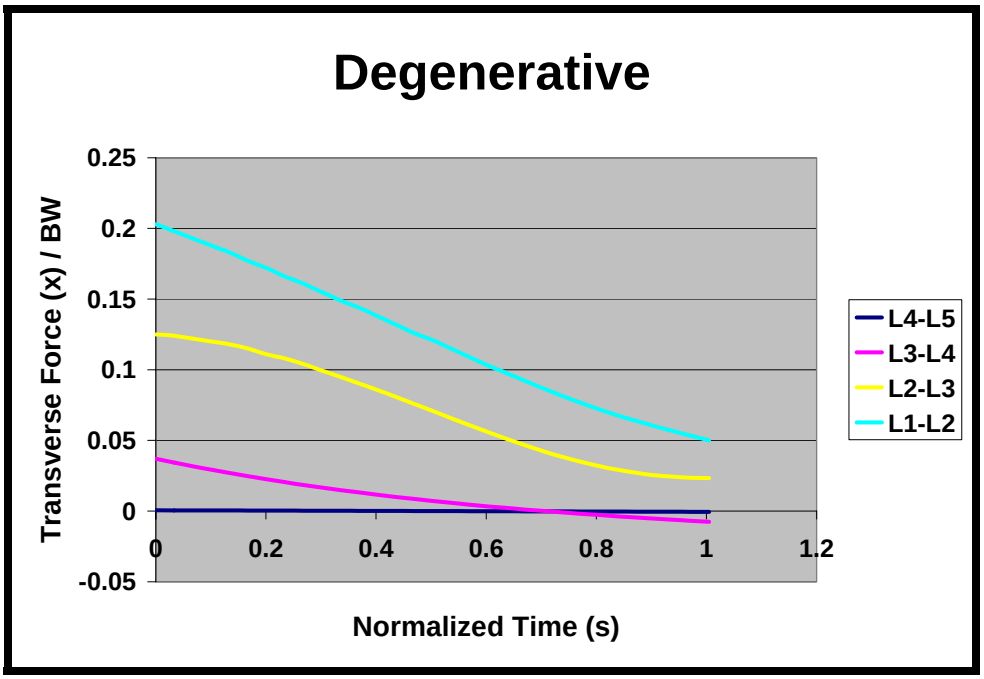

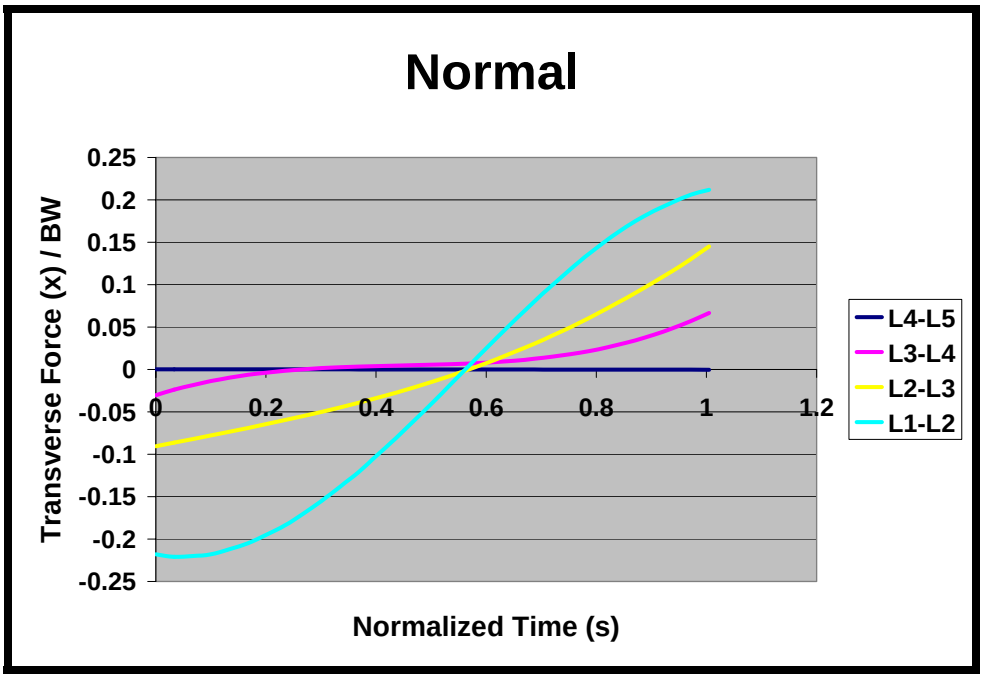

Figure B-2. Transverse forces in the x (1) direction at every level for the degenerative patient (Top) and the normal patient (Bottom).

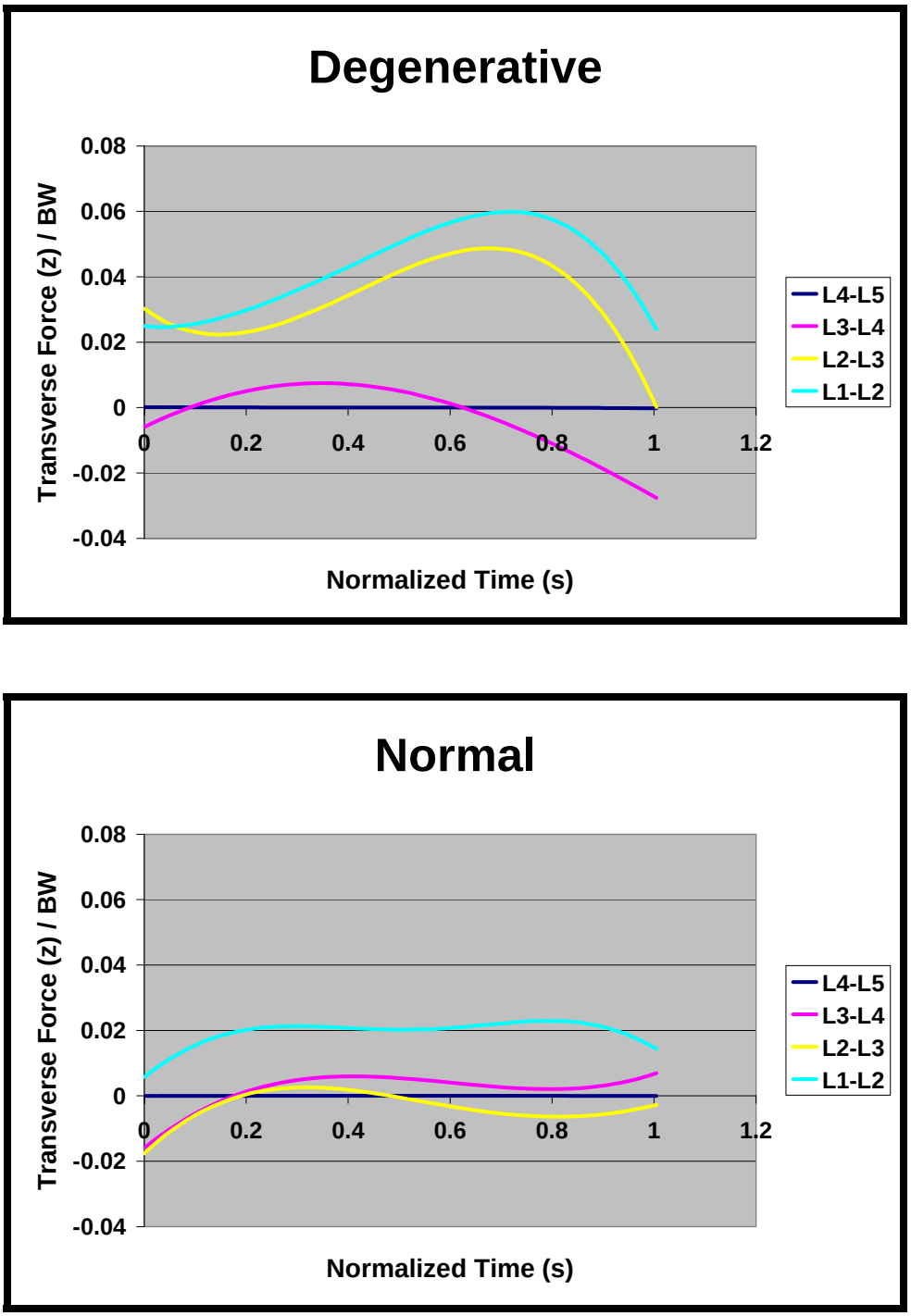

Figure B-3. Transverse forces in the z (3) direction at every level for the degenerative patient (Top) and the normal patient (Bottom).

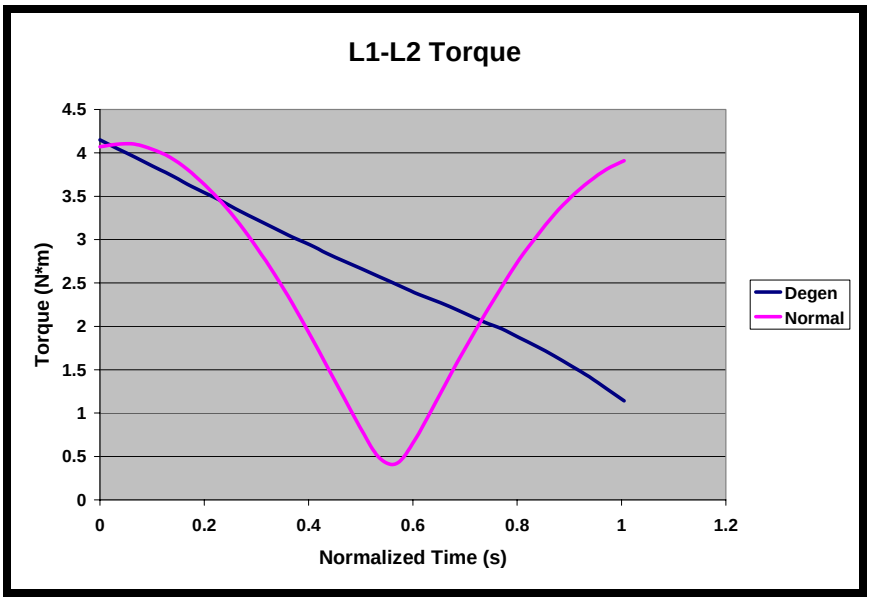

Figure B-4. Resultant torques between L1 and L2 in the degenerative patient and normal patient.

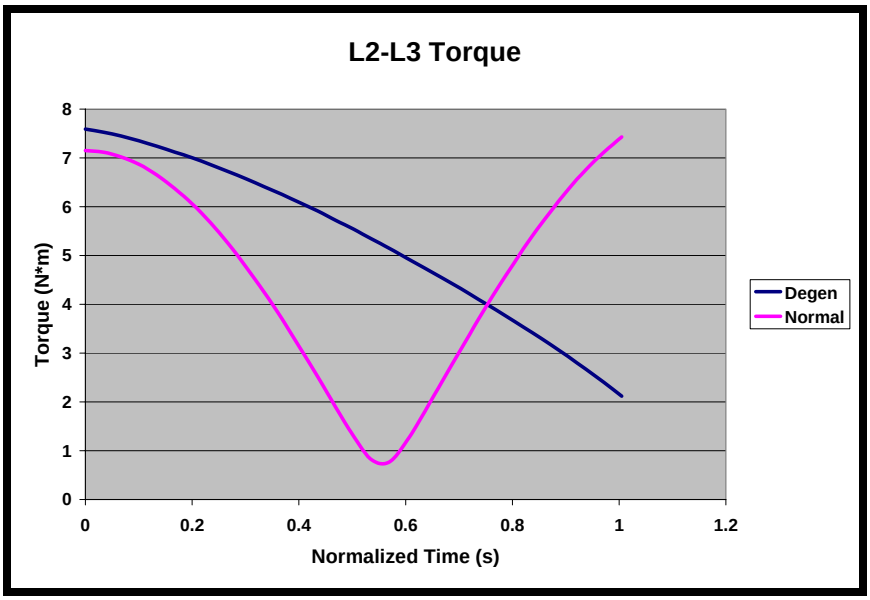

Figure B-5. Resultant torques between L2 and L3 for the degenerative patient and the normal patient.

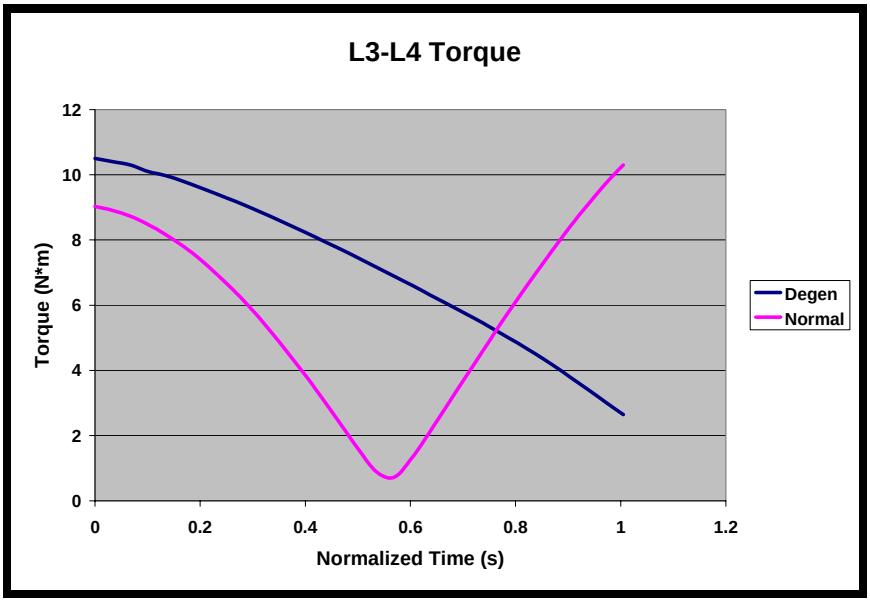

Figure B-6. Resultant torques between L3 and L4 in the degenerative patient (Top) and the normal patient (Bottom).

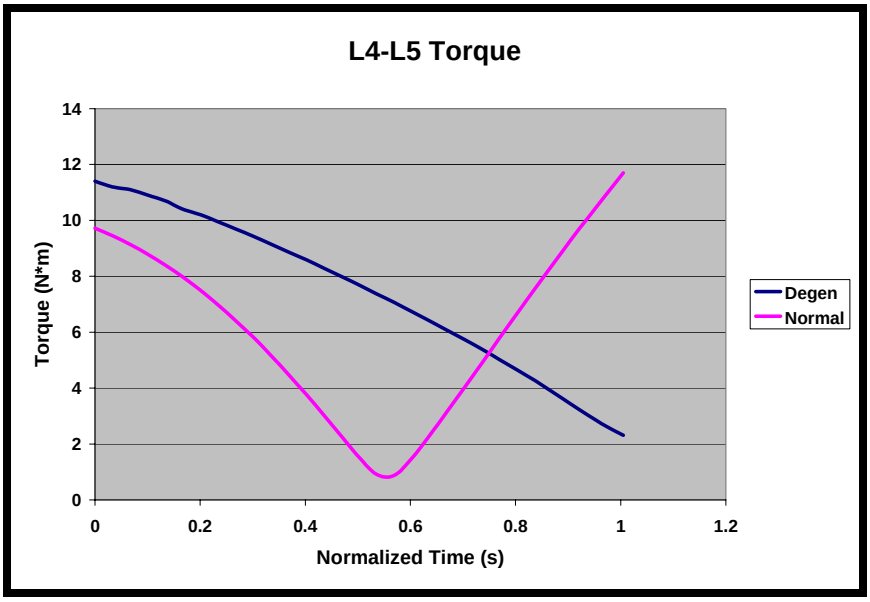

Figure B-7. Resultant torques between L4 and L5 in the degenerative patient (Top) and the normal patient (Bottom).

VITA

Shaun grew up in Knoxville and went to Farragut High School and enjoyed playing sports. He graduated from the University of Tennessee, Knoxville with a BS degree in biomedical engineering in the Fall of 2002. He received his Master's Degree in engineering science from the University of Tennessee in summer, 2005. He is either going on for a PhD, getting a job, or going to play in the NBA.